Viral infection induces oxylipin chemical signaling at the end of a summer upwelling bloom: implications for carbon cycling.

Bethanie Edwards[1*], Kimberlee Thamatrakoln[2], Chana F. Kranzler[3], Justin Ossolinski[4], Helen Fredricks[4], Matthew D. Johnson[5], Jeffrey W. Krause[6,7], Kay D. Bidle[2], Benjamin A.S. Van Mooy[4].

1- Department of Earth and Planetary Science, University of California-Berkeley, Berkeley, CA 94720, USA
2-Department of Marine and Coastal Sciences, Rutgers University, New Brunswick, NJ 08901, USA;
3- Mina & Everard Goodman Faculty of Life Sciences, Bar-Ilan University, Ramat Gan, Israel
4-Department of Marine Chemistry and Geochemistry, Woods Hole Oceanographic Institution, Falmouth, MA 02543
5- Department of Biological Oceanography, Woods Hole Oceanographic Institution, Falmouth, MA 02543
6- Dauphin Island Sea Lab, Dauphin Island, AL, USA.
7- Stokes School of Marine and Environmental Sciences, University of South Alabama, Mobile, AL 36608 USA
*Corresponding author: bethanie_edwards@berkeley.edu

Abstract/Summary (296/300-word max)

Diatoms are large phytoplankton that form the base of the marine food web and often bloom first when nutrients are injected into the surface ocean through upwelling or deep ocean mixing[1,2]. Diatoms contribute 20% of global photosynthesis[3] while disproportionately representing 40% of carbon export[4], with most export occurring along the continental margins[5]. Oxylipin chemical signaling by diatoms has been extensively studied in the Mediterranean Sea where oxylipins are linked to grazing with subsequent insidious effects on copepod reproduction[6–13]. Culture studies with diatoms have shown that stress, growth phase, and viral infection also impact oxylipin production[14–16]. This study provides insight into the role of oxylipins as biomarkers and chemical signals during viral infection of diatoms in natural communities. Biomarkers for lysis and senescence were identified in laboratory experiments and observed at elevated concentrations in meta-lipidomes collected in the California Coastal Ecosystem (CCE) where diatoms had recently been lysed by viruses[17]. Deck-board incubations with natural communities show that oxylipins stimulate sinking particle-attached and surface-ocean microbes in a dose and community-dependent manner, while inhibiting microzooplankton grazing and phytoplankton growth rates. Carbon export was two times higher at the Post-lytic site than elsewhere along the transect consistent with the viral shuttle, whereby viruses facilitate carbon export. We previously reported enhanced enzymatic activity at the Post-lytic site[17], suggestive of the viral shunt, whereby carbon is remineralized or attenuated into non-sinking dissolved organic matter. Here we layer geochemical evidence to show that lysis of oxylipin producing diatoms amplified the vertical flux of carbon from the surface ocean even in the presence of viral shunt processes. The remineralization length scale and community composition have been hypothesized as controls on shunt vs. shuttle[18–20]; our analysis provides another example of how community interactions may toggle a system between favoring shunt or shuttle.

Introduction

In 1999, Miralto *et al*. linked chemical signals produced by diatoms to decreased copepod egg viability during spring blooms in the Adriatic Sea (Northern Mediterranean)[6]. These chemical signals, polyunsaturated aldehydes (PUAs; Fig 1A), belong to the oxylipin subclass of lipids and resemble grazing defense molecules produced by higher plants. Subsequent research using diatom cultures explored the biosynthesis pathways of PUAs and other non-volatile oxylipins (NVOs)[14,15,21,22], which rely on enzymatic oxidation of polyunsaturated fatty acids, specifically C22:6, C20:5, C20:4, C16:4, and C16:3. The production of oxylipins in diatoms is generally tied to stress with studies showing relationships

between enhanced oxylipin concentrations and nutrient stress, copepod grazing, cell disruption, microzooplankton grazing, membrane permeability, virus infection and growth phase[8,10,12,16,23–26].

Oxylipin amendment experiments with cultured isolates and natural communities[27–35] (summarized in Fig. 1B) reveal a variety of cellular and ecosystem impacts. Oxylipins are largely deleterious, causing teratogenic effects on the offspring of metazoan grazers[6,7,9,10,36], deterring microzooplankton grazing by microzooplankton[31–33,37], and stunting the growth of eukaryotic phytoplankton competitors[27,31]. Specifically, PUAs are also a fundamental component of a nitric oxide-based, stress surveillance system whereby diatoms sense and respond to biotic and abiotic stressors, which can lead to the activation of programmed cell death at threshold concentrations[29]. At sub-lethal concentrations, PUAs can desensitize diatom cells to physiological stress and fortify cellular responses for growth and survival[29]. Lastly, PUAs have been found to be stimulatory to particle-associated bacteria and diatom epibionts in sublethal doses (1-10 µM in the Atlantic; 13-18 µM in culture), while free-living bacterial isolates tend to be inhibited at concentrations as low as 3 µM[28,35]. PUA concentrations high enough to deter microzooplankton grazing and stimulate particle-associated communities have been observed in the water column in the Mediterranean Sea[7,23,25,27,38] , within sinking particles in the Atlantic[35], and within suspended particles in the Pearl River Estuary, China[39] (Table S1; Fig. S1).

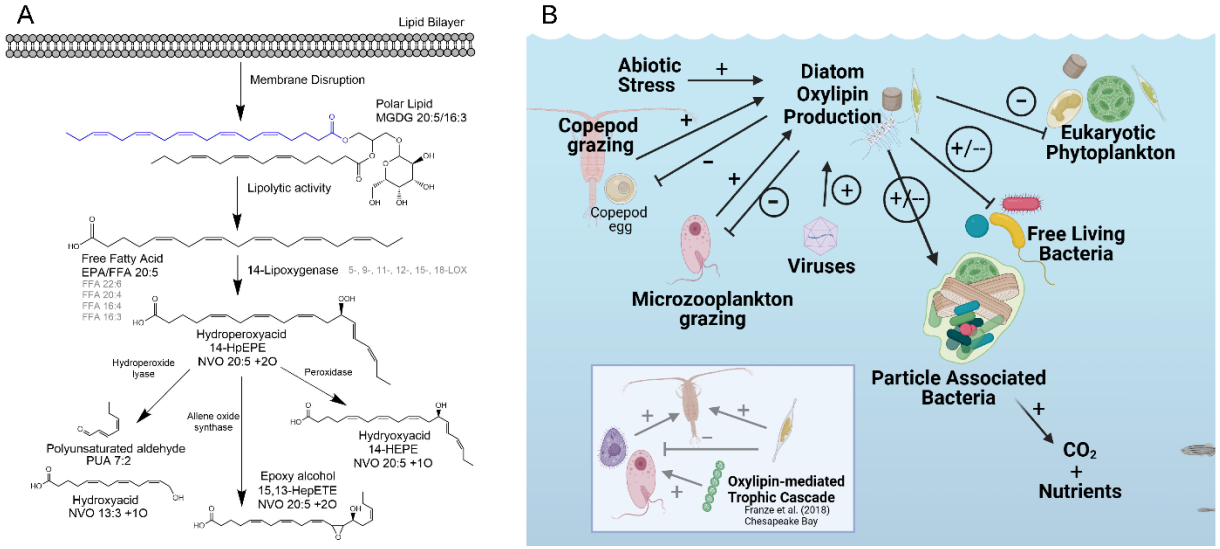

Figure 1. Diatoms in the ocean biosynthesize oxylipins from membrane lipids, which act as chemical signals impacting growth, behavior, cell fate, and biogeochemistry. A) Oxylipin biosynthesis pathway proposed for the 14-lipoxygenase enzyme acting on eicosapentaenoic acid which was lipolytically cleaved from the membrane lipid, MGDG 20:5/16:3 (monogalactosyldiacylglycerol). A hydroperoxy acid is the first compound produced, 14-hydroperoxy eicosapentaenoic acid (14-HpEPE). Enzymes downstream of LOX act on the hydroperoxy acid to produce a plethora of oxylipin compounds. Here we include other common lipoxygenases which add a hydroperoxy group (-OOH) at the specified carbon position along the fatty acid chain. **B)** Assessments of oxylipin bioactivity in surface ocean ecosystems based on culture amendment experiments and deck-board incubations[6,7,12–16,26–28,31,32,35,40,41]. Arrows denote the directionality of response and +/- denotes stimulation or inhibition, respectively (depending on concentration). Circled responses indicate interactions explored in this study. Inset shows the trophic cascade mediated by PUAs in a natural population from the Chesapeake Bay, where oxylipins decreased grazing of microzooplankton like dinoflagellates (pink flagellate) and ciliates (purple ciliated cell) on diatoms but increased grazing on cyanobacteria (green chain-forming cells) and increased copepod grazing on both diatoms and ciliates[31].

We previously presented a detailed comparison of the suite of oxylipins produced by three different *Chaetoceros* diatom host-virus systems, highlighting the unique oxylipins produced by each host-virus

pair, and focusing on compounds with known allelopathic effects on meso- and microzooplankton grazers[16]. *Chaetoceros* species are abundant in natural diatom communities in the CCE and the most abundant diatom in the global TARA Oceans dataset[17,42–45]. Virus infection is an important loss term for phytoplankton in the marine environment with mortality rates on par with grazing across the North Atlantic and Southern Ocean[46,47]. Given lipids have been used as diagnostic biomarkers for viral infection of the coccolithophore, *Gephyrocapsa huxleyi*[48], including in natural populations across the North Atlantic[49], we sought to 1) explore oxylipins as biomarkers of viral infection in diatoms and 2) test the ecological relevance of oxylipin chemical signaling during infection. We took a two-pronged approach, using a laboratory model system with three diatom host-virus pairs[16,50–52]and analysis of meta-lipidomic data from diatom assemblages in the CCE.

Three phytoplankton patches with natural diatom populations were found to be in different stages of the bloom lifecycle and viral infection (Active Infection, Post-lytic, and Non-blooming) in a 2013 field study along the CCE and established a link between viral infection and silicon limitation[17]. Our analyses showed that dissolved oxylipins in the CCE meta-lipidome were more abundant at a Post-lytic sites than at Active Infection sites or a Non-blooming sites dominated by dinoflagellates. Five of the oxylipin biomarkers from control, laboratory infection experiments were more abundant *in situ* at the Post-lytic site coinciding with higher bacterial ectoenzyme activity[17] and higher Si-stress[17,43] compared to the Active Infection site. Deck-board incubations exposing surface and sinking particle-associated microbial communities to exogenous oxylipins suggest that they impact grazing, growth, and organic matter cycling by marine microbes. At the same time, sediment traps and satellite data confirm the higher oxylipin post-lytic siters also had higher magnitude and efficiency of carbon export.

Results and Discussion

Viral Infection and mortality biomarkers identified in culture experiments

Two diatom species (*Chaetoceros tenuissimus* strain 2-10 *and C. socialis* strain L-4) served as hosts in laboratory infection experiments with three taxonomically distinct viruses: a single-stranded DNA (ssDNA) virus (CtenDNAV) and a single-stranded RNA (ssRNA) virus (CtenRNAV), both infecting *C. tenuissimus;* and a ssRNA virus (CsfrRNAV), infecting *C. socialis.* Control and infected treatments were sampled for lipidomics and cell concentration over 3-4 days post infection (dpi; Fig. 2A, S2). Samples were categorized based on the growth phase (Exponential, Stationary, and Decline) and dissolved lipidomes were annotated as described in Edwards et al.[16]. We evaluated the general lipidomic response across the three host-virus pairs to elucidate viral infection and senescence responses shared across the genus *Chaetoceros.*

The dissolved lipidome (<0.2 μm) represents small and often oxidized lipids that are more soluble than hydrophobic storage lipids or polar membrane lipids. High Resolution Accurate Mass-Mass Spectrometry (HRAM-MS) paired with reverse phase ultra-high performance liquid chromatography analysis was used to analyze the dissolved lipid extracts and reference standards (Table S2). To address specific questions about oxylipin abundance and diversity, we focused on the 156 compounds confidently annotated as free fatty acid (FFA) precursors of oxylipins and NVOs. Equal weight was given to high and low abundance compounds by mean-centering and log-transforming the peak area data after normalizing to the volume filtered and the recovery of an internal standard (Supplemental File 1). A comparative -omics scheme[53,54]

was applied to the resulting dissolved oxylipin profiles using hierarchical clustering analysis and multivariate analysis to determine significant biomarkers of viral infection, stress, and death.

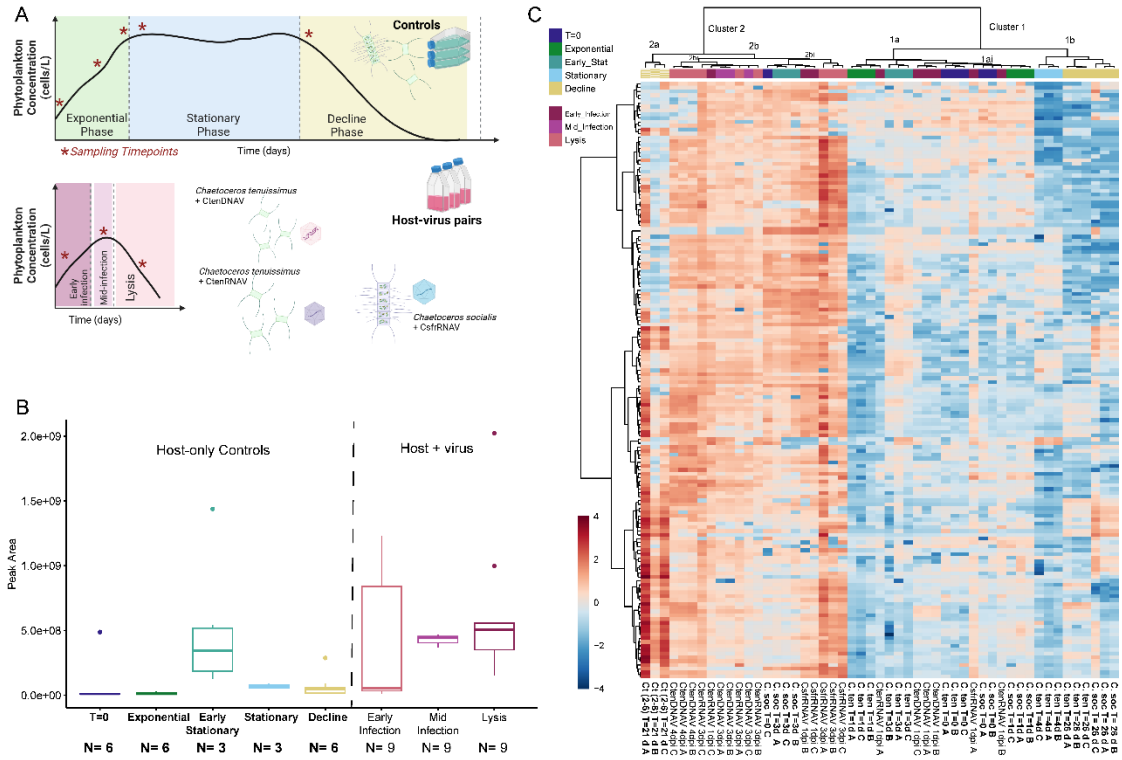

Figure 2. Virus infection of diatoms leads to the release of oxylipins and free fatty acids into the dissolved organic matter pool. A) Experimental design showing a representative growth curve of the host-only control and representative time course of infection for three diatom host-virus pairs: The approximate sampling timepoints are noted with red asterisks. The actual growth curve of each triplicate treatment can be found in Fig. S2. **B)** Box and whisker plots of the average peak area of oxylipins and free fatty acids in the dissolved lipidome for host-only controls and the stage of infection averaged across all three viruses. The edges of the box indicate the 1st to 3rd quartile range; error bars represent the standard deviation with outliers noted by dots. **C)** Heatmap of the oxylipidome (Oxylipins + FFA) from the *Chaetoceros* viral infection experiments showing the relative abundance of each compound relative to its mean concentration across all samples with red indicating a relative increase and blue a relative decrease, reported as a log fold change. Colored bars above the heatmap denote the growth phase and infection stage as indicated. The samples on the X-axis and compounds in the Y-axis are ordered based on the dendrogram created using Ward clustering. Important clusters of samples that are discussed in the text are labeled on the dendrogram. Timepoints as labeled by color at the top of the heatmap and individual samples are labeled at the bottom of the heatmap. Controls are labeled with the host name, day sampled after transfer, and triplicate identifier, A, B, or C. Infected samples are labeled with the virus, days post infection (dpi), and triplicate identifier, A, B, or C.

Chaetoceros produced the highest absolute abundance of FFAs and NVOs (*i.e.*, non-PUA oxylipins) during the later stages of viral infection (mid-infection and lysis) and in early stationary phase in controls (Fig. 2B-C). Hierarchical clustering analysis split the data into two clusters revealing distinct lipidome structures between the cells lysing due to viral infection (Cluster 2) and the aging, control treatments (Cluster 1; Fig. 2C). Within Cluster 2, 15 of 22 samples are infected, and within Cluster 2bi, all 10 samples are from mid-infection and lysis of *C. tenuissimus*. This suggests that *C. tenuissimus* lipidomes from virocells are more similar to one another than to other species infected with similar viruses.

Triplicates from two controls grouped with the T= 3 and 4 dpi virus samples, stationary phase *C. socialis* and declining *C. tenuissimus* from a different strain (2-6) than the CtenDNAV and CtenRNAV host (2-10). The C. *tenuissimus* host lipidome (2-10) grouped with the declining *C. socialis* host control in Cluster 1. Although *C. tenuissimus (2-6)* was not used as a host in our virus infection experiments, it was included in our metanalysis as an outgroup and a unique lipidomic signature, forming its own subgroup within Cluster 2 (Fig. 2C, Cluster 2a.). *C. socialis* showed elevated oxylipins in stationary phase with an overall lipidome most similar to CsfrRNAV infected cells (Fig. 2C, Cluster 2bii samples labeled C. soc T=3 d).

Cluster 1 was enriched with control samples (23 of 29 samples). The declining control samples from *C. tenuissimus* (2-10) and *C. socialis* clustered with stationary phase *C. tenuissimus* (2-10), and showed lower relative abundances of most oxylipins observed in the experimental dissolved meta-lipidome (Fig. 2C- Cluster 1b). The only virus infected treatments in Cluster 1 are early infection samples (T= 1 dpi; 6 of 29 samples).

The observed strain-level variability in the relative abundance and chemical diversity of oxylipins produced was consistent with Wichard *et al.*, which surveyed PUA production in 50 strains of phytoplankton (primarily diatoms)[16,22]. Ribalet *et al.* had previously established that the diatoms, *Skeletonema* and *Thalassiosira,* increase the production of free fatty acid and PUAs as they reach stationary phase and even more so under nutrient stress, particularly Si-limitation[14,15]. Our method was not optimized for PUA quantification, but rather for the pool of less volatile compounds adjacent and upstream of PUA production (Fig. 1A), showing plasticity in the range of non-volatile oxylipins produced by *Chaetoceros* diatoms under different growth conditions.

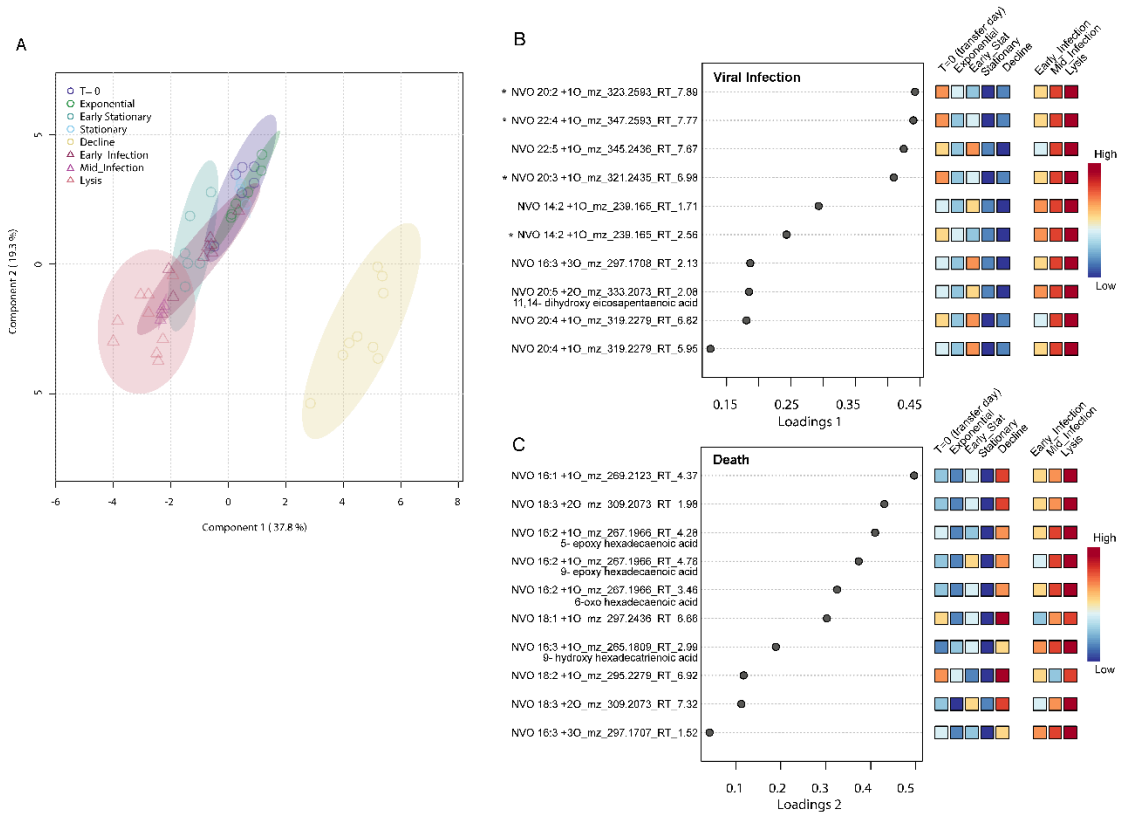

Fig 3. Biomarkers for virus infection and general cell death of diatoms A) Loadings of the dissolved lipidome samples on Component 1 and 2 of the sparse PLSDA. Control samples are represented by a colored circle corresponding to the time of sampling (T=0, exponential, early stationary, stationary, and decline) and infected treatments are represented by pink triangles of various shades. show growth phase and viral infection lead to distinct changes in the dissolved lipidome. **B-C)** The significant compounds assigned to Components 1 and 2 by the sPLS-DA, their loadings on either component are shown as a dot-plot and the heatmap shows the average relative abundance of each compound across each timepoint. **B)** Component 1 separates the viral infection lipidomes from the decline lipidome. **C)** Component 2 captured the signal from cell death more generally.

Sparse Partial Least Squares - Discriminant Analysis (sPLS-DA) was used to distill the dataset down to the twenty most distinctive features that best differentiate time-points and treatments from each other, in hopes of identifying discrete biomarkers for viral infection or general cell death (Fig. 3). Compounds that increased over the course of infection and were most abundant during lysis were assigned to Component 1 (Fig. 3B). The strongest viral biomarkers were compounds that were only abundant in the control on the transfer day (T=0) and increased with viral infection (NVO 20:2 +1O, NVO 22:4 +1O, NVO 20:3 +1O, and NVO 14:2 +1O; Fig. 3B). While the other Component 1 compounds (a different NVO 14:2 +1O isomer, NVO 22:5 +1O, NVO 16:3 +3O, two isomers of NVO 20:4 +1O, and 11,14-dihydroxy eicosapentaenoic acid) increased with infection but were present in early stationary phase as well. Compounds that were more associated with a general death response (*i.e.*, high during decline of the control and during lysis of the infected cultures) were assigned to Component 2 (Fig. 3C).

Twelve of the twenty significant oxylipins were close analogs of known allelopathic compounds produced by diatoms that negatively influence copepod reproductive success in the Mediterranean Sea and microzooplankton grazing in the laboratory[8,10,25,33] (Table S3). These results suggest viral infection

triggers a pulse of chemical signaling via oxylipins that is distinct from the shared suite of oxylipins produced by dying, uninfected cells. This chemical signaling could impact trophic interactions and the associated biogeochemistry. We tested this hypothesis by analyzing a dissolved lipidome dataset from a field study in the California Coastal Ecosystem (CCE), where we previously characterized different stages of viral infection and conducted deck board amendment experiments with different communities using a range of oxylipin concentrations.

Bloom decline and viral infection are linked to oxylipin production and efficient export *in situ*

Biogeochemical evidence of bloom decline and enhanced export

The DYEatom cruise (June 27th – July 6th, 2013; *R/V Point Sur*) occupied nine stations within the CCE upwelling zone. The physical oceanography, phytoplankton composition, Si-stress, and infection state have been previously characterized[17,43]. Briefly, near-shore stations outside Monterey Bay were dominated by diatoms, particularly *Pseudo-nitzschia*, that were characterized as being actively infected (Active Infection) at the time of sampling. Near-shore stations by Point Reyes were also diatom-dominated but were more diverse in species composition (see Fig. 1c in Kranzler et al.[17]); they were further characterized as having undergone a recent viral-mediated mortality event (Post-lytic). Here, we present an analysis of the dissolved meta-lipidome from these two contrasting regions, along with two offshore stations that were dominated by dinoflagellates that serve as functional controls (Fig. 4, 5, S3).

Mean net primary productivity (NPP) in the region during our occupation was derived from satellite data and the CAFE algorithm[55] (Fig. 4B-C). This analysis showed that we sampled an Active Infection at the Monterey Bay sites (Fig. 4E), coincident with a peak in NPP (Fig. 4B). The Post-lytic Point Reyes site had the lowest NPP at the time of sampling, consistent with a decline in productivity and diatom bloom demise. *In situ* measurements of chlorophyll, a common proxy for phytoplankton, further supported the distinction between sampling sites with concentrations between 8-18 μg L^{-1} in Monterey Bay and 3.9- 7.5 μg L^{-1} at Point Reyes[43].

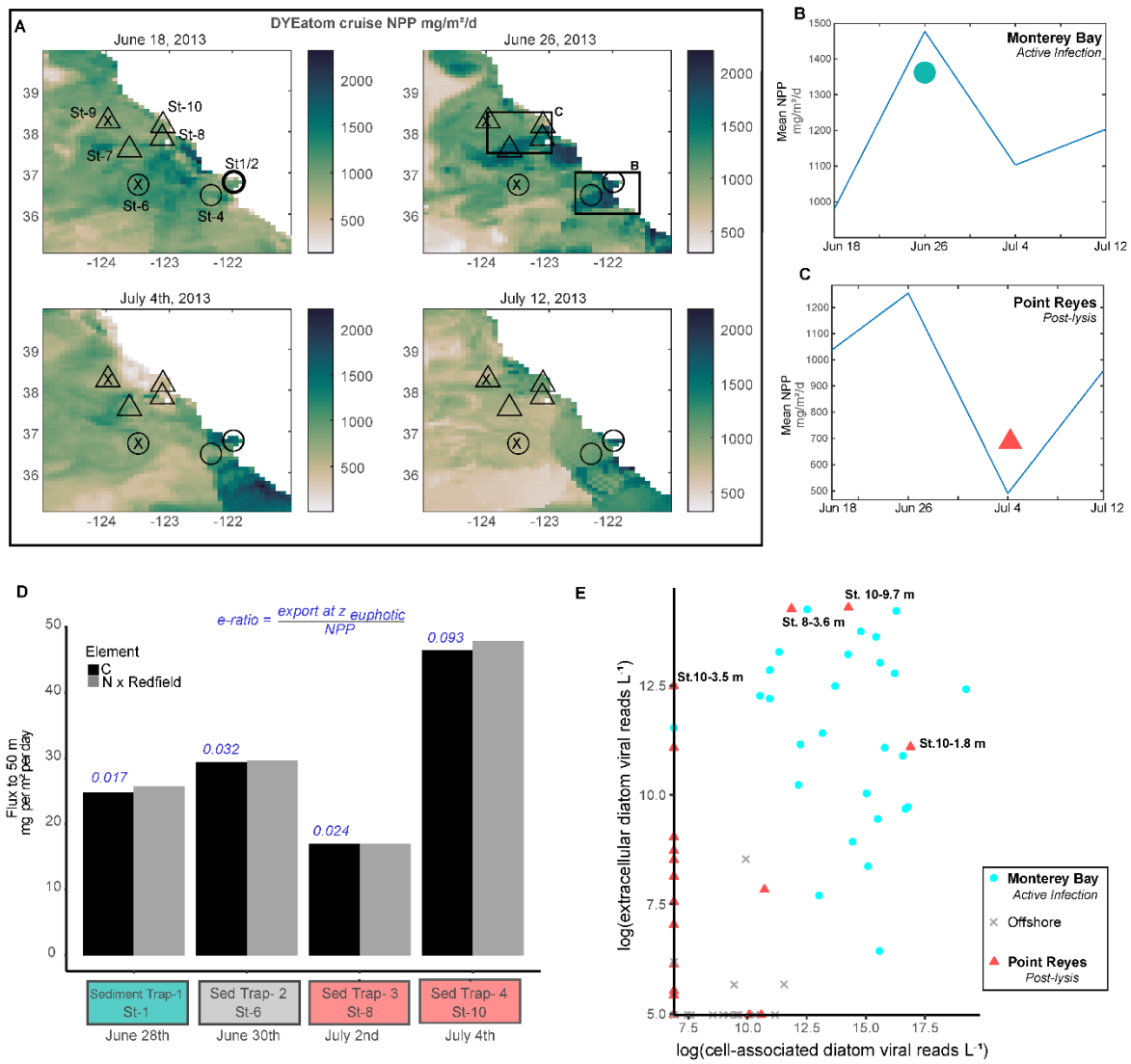

Figure 4. Diatom-virus dynamics, net primary productivity, and export signatures. A) A map of sampling sites during the DYEatom cruise (June 27 -July 6, 2013) and associated net primary productivity (NPP; dark green gradient) integrated over 8-day bins from June 18, 2013 to July 12th, 2013 using the CAFE Model[52] of MODIS satellite data. Open circles indicate Monterey Bay stations; open triangles indicate Point Reyes stations. The stations marked with an 'x' indicate non-bloom site outside the upwelling filaments. Time course of the mean ocean NPP within the 1° latitude by 1° longitude rectangles drawn around **B)** Monterey Bay and **C)** Point Reyes. Filled symbols represent when Monterey Bay (cyan circle) and Point Reyes (coral triangle) were sampled. **D)** Particulate organic carbon (POC; black bars) and particulate organic nitrogen (PON; grey bars scaled to C by multiply by 6.6) flux to 50 m, as determined using sediment traps deployed at four stations over different stages of bloom decline. The blue text above each black bar indicates the export ratio calculated from the POC data and the NPP satellite estimates. **E)** Data reproduced from Kranzler *et al.* (2019)[17] showing cell-associated diatom virus and extracellular virus copy numbers for three contigs identified as diatom RNA viruses similar to those used in culture experiments from Fig. 3[50,51].

Sediment traps were used to quantify carbon export out of the mixed layer (to 50 m) and calculate export efficiency as an apparent e-ratio (export at $Z_{euphotic}$/NPP; Fig. 4D). The carbon flux in Monterey Bay was similar to the offshore, non-diatom dominated station (24.7 and 29.3 mg m^{-2} d^{-1}, respectively), although the latter had a ~2-fold higher e-ratio of 0.032 (compared to 0.017). The highest carbon flux (46 mg m^{-2}

247 d^{-1}) and highest e-ratio (0.093) were observed at the Post-lytic Point Reyes site on July 4th (St. 10),
248 suggesting export efficiency increased as viral infection and bloom declined progressed. The lowest
249 measured carbon export flux was two days prior at a nearby station also characterized as Post-lytic St. 8),
250 reflecting the time-resolved connection between infection dynamics and episodic carbon export[56–59].
251 Unlike St. 8, St. 10 still had detectable levels of intracellular virus (Fig. 4E), which may help explain
252 differences in export. St. 10 was closer to the origin of upwelling and the populations appeared to be
253 earlier in the lytic process while St. 8 was more offshore and further along in the lytic cycle. It is possible
254 that St 8 was sampled after an export event had already occurred, as is evidenced by the removal of
255 viruses from both the free-living and cell-associated fraction presumably by adsorption onto particles (a
256 known sink for viruses from the water column[60]).
257
258 We recognize that the type of sediment trap deployed, a surface-tethered net trap, is not as quantitative as
259 a particle interceptor trap (PIT) array or neutrally buoyant trap in determining quantitative fluxes[61];
260 consequently, we may be underestimating export. However, given the same net traps were used across all
261 stations, these caveats (high precision, low accuracy) should be uniform, allowing intercomparison of
262 export between sites. Furthermore, the highest e-value measured (0.093) notably aligns with regional
263 estimates from Henson *et al.* derived as a function of SST[62,63] although it is lower than an estimated
264 global average e-ratio of 0.17[62] and regional estimates from other models based on satellite color and
265 food web dynamics.
266
267 ***Dissolved meta-lipidome reveals abundance of death and virus biomarkers in Post-lytic communities***
268 Within the dissolved meta-lipidome, 175 compounds were annotated as oxylipins or free fatty acid
269 precursors (Supplemental File 2). The Post-lytic site had a higher relative abundance of dissolved organic
270 lipids compared to the Active Infection or non-bloom sites, especially on July 4th (St 10; Fig. 5A). The
271 Active Infection and Post-lytic lipidomes were more similar to one another than to the non-bloom
272 lipidomes, clustering together in the sample dendrogram (Fig. 5A). sPLS-DA was used to identify the
273 most significant features in the dissolved lipidome for differentiating between the bloom states.
274 Component 1 represented 55.1% and Component 2 represented 19.7% of the respective variability in the
275 data (Fig. 5B), with the former containing compounds significantly associated with the Post-lytic stage of
276 infection (Fig. 5C) and the latter compounds more associated with Active Infection (Fig. 5D).
277
278 Three general death biomarkers and two viral lysis biomarkers from the *Chaetoceros* lab experiments
279 were amongst the most significant compounds associated with the Post-lytic site (Fig. 5C, bold and red
280 compounds, respectively; Table S5). The general death biomarkers 9-hydroxy hexadecadienoic acid (9-
281 HHDE), 9-hydroxy hexadecaenoic acid (9-HHME), and 9-oxo hexadecaenoic acid (9-oxoHME) all
282 belong to the 9-LOX pathway acting on 16:n fatty acids previously observed in *Skeletonema marinoi* and
283 *Thalassiosira rotula* (Table S3). The abundance of the viral lysis biomarkers, 20:4 +1O and 22:5 +1O,
284 was too low to gain positional information from ms^2 fragmentation, but a retention time model indicates
285 these oxylipins are hydroxy acids similar to those made by *T. rotula*, *Stephanopyxis turris*, and
286 *Leptocylindrus* (Table S3; Supplemental File 3).
287
288 The most significant compounds in the dissolved lipidome from the Active Infection site were eight
289 highly oxidized C22:n oxylipin isomers, the FFA and oxylipin precursor, hexadecatetraenoic acid
290 (C16:4), and a C18:4 oxylipin (Fig 5D). While less oxidized DHA oxylipins, 22:5 +1O and 22:4 +1O,

were prominent viral infection biomarkers in lab infection experiments (Fig. 3B), the highly oxidized +3O and +4O compounds associated with the Active Infection site are unique for marine systems (Fig 5D). However, C22:n oxylipins alone may not be specific enough to be indicators of viral infection. For example, C22:n biosynthesis pathways have been studied in *Leptocylindrus* diatoms showing that, in response to sonication, 15- and 18-lipoxygenases are employed to make +1O and +2O C22:n oxylipins[64]. We previously observed C22:6 +2O oxylipins produced in culture experiments feeding *Phaeodactylum tricornutum* to the dinoflagellate *Oxyrrhis marina* [33]. Hydroxy and epoxy-hydroxy DHA derived oxylipins have been found in other natural systems, constituting approximately 20% of the total NVO pool from January to December 2017 at the LTER-MareChiara in the Mediterranean Sea where particulate oxylipin concentrations were positively correlated with diatom density[25]. The highly oxidized nature (+3O and +4O) of the C22:n oxylipins at the Active Infection site may be related to the stress-level of the community and should be further investigated as biomarkers for infection vs. +1O and +2O C22:n oxylipins, which may be more general stress biomarkers.

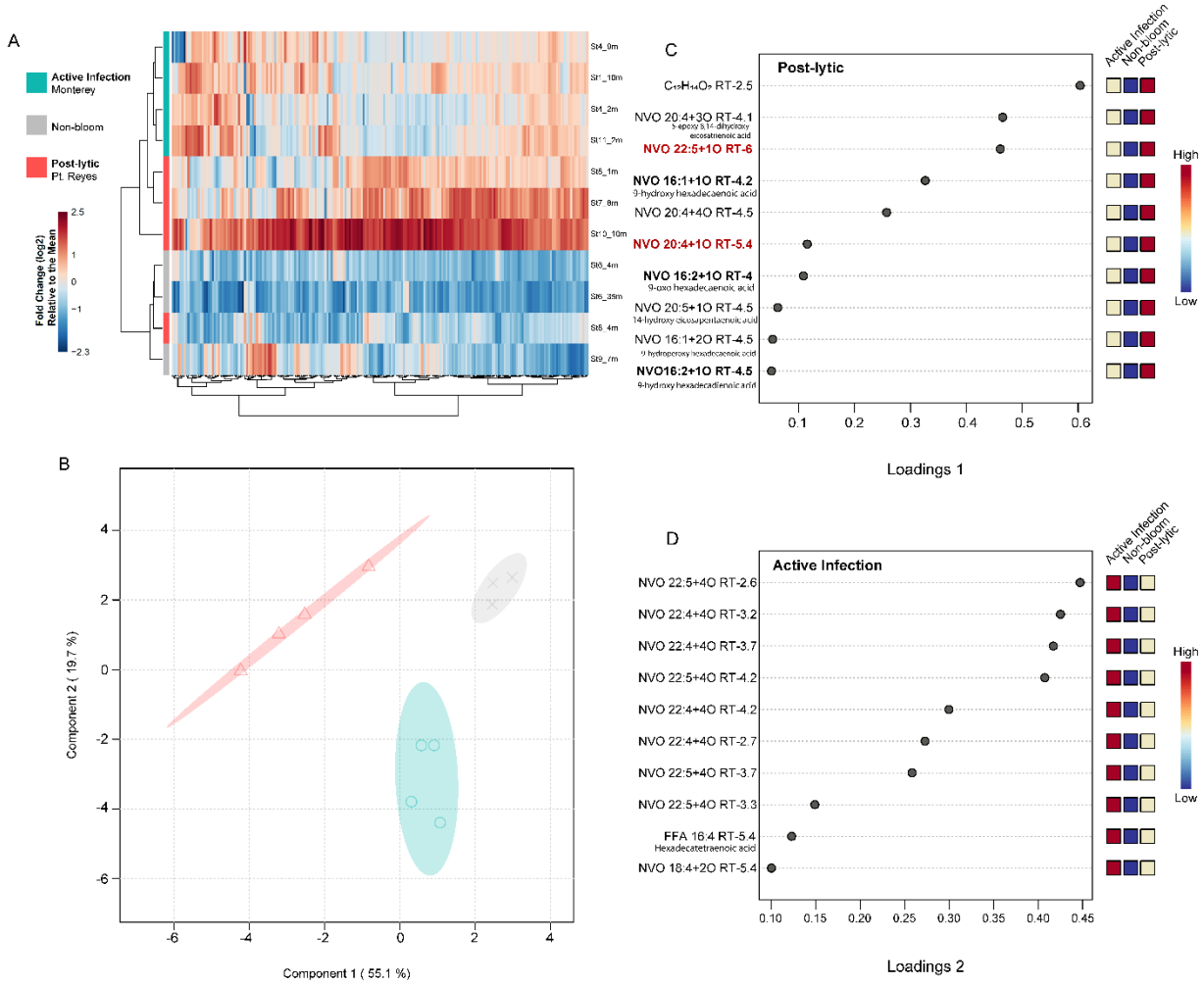

Figure 5. Oxylipin biomarkers of infection state from the DYEatom meta-lipidome. A) Heatmap showing the relative abundance of 175 compounds identified as free fatty acids and oxylipins in eleven dissolved lipidome samples from the DYEatom cruise. Samples on the X-axis (lipid compounds) and Y-axis (station and depth) are organized by similarity depicted by the Ward clustering in the dendrogram. **B)** Loading of the dissolved meta-lipidome samples on Components 1 and 2 derived from sPLS-DA for samples collected at Point Reyes (coral

triangles), Monterey Bay (cyan circles), and non-bloom sites (grey x). The 95% confidence intervals (colored ellipses) for the three bloom states do not overlap. Component 1 (55.1% of the variability in the data) distinguishes the post-lytic samples from the other two categories; Component 2 (19.7% of the variability in the data) describes active infection. **C- D)** The ten compounds from the dissolved meta-lipidome used to derive **C)** Component 1 and **D)** Component 2 in the sPLS-DA. Compounds are ordered by their loading as noted by the dot-plot. Heatmaps show the average relative abundance of each compound in the dissolved meta-lipidomes from each bloom state. Compound annotations in red text are biomarkers of viral infection in *Chaetoceros* cultures (Fig. 3B), while those in bolded black text are more general cell death biomarkers (Fig. 3C).

Oxylipins function as chemical signaling across trophic levels in the California Current

Similar to the compounds identified in laboratory experiments, NVOs associated with Post-lytic stage of infection at Point Reyes are also known to have allelopathic effects on microzooplankton grazers in culture and copepods at sea[8,10,33] (Table S5; Fig. 5C). An isomer of the NVO 20:4 +3O oxylipin, annotated as a 5-epoxy-8,14-dihydroxy eicosatrienoic acid, was associated with dinoflagellate grazing deterrence and chronic stress in *P. tricornutum* experiments[33]. Furthermore, the C16:1, C16:2, C20:4 and C20:5 oxylipins from the Post-lytic site have been observed in diatom blooms in the Adriatic Sea that are detrimental to copepods[8,33].

Unlike grazers, the effects of oxylipins on eukaryotic phytoplankton and bacteria have only been widely studied using commercially available PUAs, not NVOs[23,27,28,30,34,35]. NVOs are upstream in the oxylipin biosynthetic pathway from PUAs (Fig. 1A) and tend to be toxic at lower doses than PUAs when tested against microzooplankton grazers in the laboratory[33] and copepods at sea[8,10,13]. To assess the role of NVOs and PUAs in signaling across trophic levels, we conducted deck-board incubations of surface assemblages and sinking particle-associated microbes treated with exogenous PUAs and NVOs (Fig. 6) and assessed trends in oxylipin concentration and microbial metabolism.

Negative feedback loop between oxylipins and grazing

A mixture of PUAs—heptadienal, octadienal, and decadienal—had differential effects on natural microbial communities from the California Current. PUAs inhibited microzooplankton grazing and phytoplankton growth (Fig. 6A-C), but stimulated hydrolytic enzyme activity (peptidase and phosphatases) in surface communities and sinking particles (Fig 6D-H). A map of grazing, growth, and a proxy for oxylipin concentration (total peak area of oxylipins and FFA in the dissolved lipidome) across the study site showed the highest oxylipin concentrations co-occurred with the lowest grazing rates and the lowest phytoplankton growth rates (Fig. S4), consistent with laboratory-based interactions[33].

The relationships between oxylipin concentration, grazing and growth across the cruise sites reflect the dose dependence of the allelopathic effects of oxylipins and the community's threshold response to these chemical cues. Excluding the highest oxylipin concentration, a positive relationship between the oxylipin concentration proxy and phytoplankton growth was observed (Fig. S5 C). The highest oxylipin concentrations occurred at the Post-lytic Point Reyes site where the oxylipin threshold for inhibiting phytoplankton had been crossed, resulting in negative growth rates (Fig. S4 A, D).

A negative feedback loop between grazing and oxylipin production was observed, whereby grazing induces oxylipin production, which further inhibits grazing (Fig. S5 D). The lowest oxylipin concentrations were observed at stations with low grazing rates. Subsequently, a negative correlation between grazing and oxylipin concentrations was observed at the four stations with the highest oxylipin

concentrations once the threshold concentration for allelopathy had been surpassed (Fig. S5 D). Several studies have documented synergy amongst various oxylipins, whereby the presence of multiple oxylipins leads to a lower effective concentration[11,13,65]. Thus, the higher diversity of lipids at the Post-lytic sites compared to the Active Infection sites (Table S6 and S7) may also contribute to the comparatively lower grazing rates (Fig. S4).

Dose-dependent PUA signaling in surface and sinking particle-associated microbial communities

We tested the sensitivity of surface and sinking particle-associated microbial communities to oxylipins by exposing them to a range of concentrations based on thresholds observed in the literature (Fig. S1; Materials and Methods). Depending on the bloom state and community, the response to exogenous oxylipins varied with shifting effective concentration thresholds and sign of response (negative vs. positive). At the Active Infection and Post-lytic sites, where background oxylipin concentrations were relatively high, addition of 100 μM PUAs to sinking particle-associated communities increased phosphatase activity and inhibited peptidase activity (Fig. 6F,H). The communities on particles collected from the lower-oxylipin dinoflagellate-dominated, non-bloom site (St 6) were inhibited for both enzymes after exposure to 100 μM PUA, but stimulated by a 10 μM addition (Fig 6G). Thus, the microbial communities that had prior exposure to oxylipins were more tolerant to exogenous oxylipin additions. Our findings agree with experiments conducted across the Pacific in the South China Sea showing stimulation of particle-associated communities in response to 10-100 μM PUAs[34]. The threshold of inhibition was lower in particle-associated communities from the Atlantic, where inhibition of enzyme activity, respiration, and bacteria growth was observed at 100 μM[35] and stimulation between 1 and 10 μM PUA addition. The community dependent response to PUAs—inhibition of both peptidase and phosphatase activity on particles collected from non-blooming sites at 100 μM (Fig 6G) —is consistent with a screening of 33 bacterial isolates showing stimulation only amongst strains known to be epibionts of diatoms[22]

In surface microbial communities from the Active Infection site, peptidase activity was stimulated and phosphatase activity was inhibited at 10 μM PUA (Fig 6D). Unfortunately, we did not replicate the 10 μM PUA treatment at the other sites; so it is unclear whether non-blooming and Post-lytic surface ocean communities are more, less or equally sensitive. This oxylipin stimulation of surface ocean microbes lies in contrast to a previous study in the NW Mediterranean that found a significant decrease in single cell activity for a subset of the bacterial community in response to nM concentrations of PUAs[66]. Another study testing daily 1-2 μM PUA additions in 21-day mesocosms found no effect on microbial composition in response to PUAs alone but did see a difference in bacterial community structure with time and in the two mesocosms that ended up with different strains of *Skeletonema* blooming after nutrient addition[67]. We previously reported enhanced peptidase activity at the Post-lytic site likely reflecting the stimulatory effect of oxylipins on enzyme activity[17]. Culture studies show enhanced peptidase activity in infected *Chaetoceros* cells compared to controls and more peptidase activity, but less growth in bacteria exposed to CtenRNAV lysate compared to CtenDNAV lysate[20], introducing the caveat that stimulation may not translate to growth or secondary production by the bacterial community.

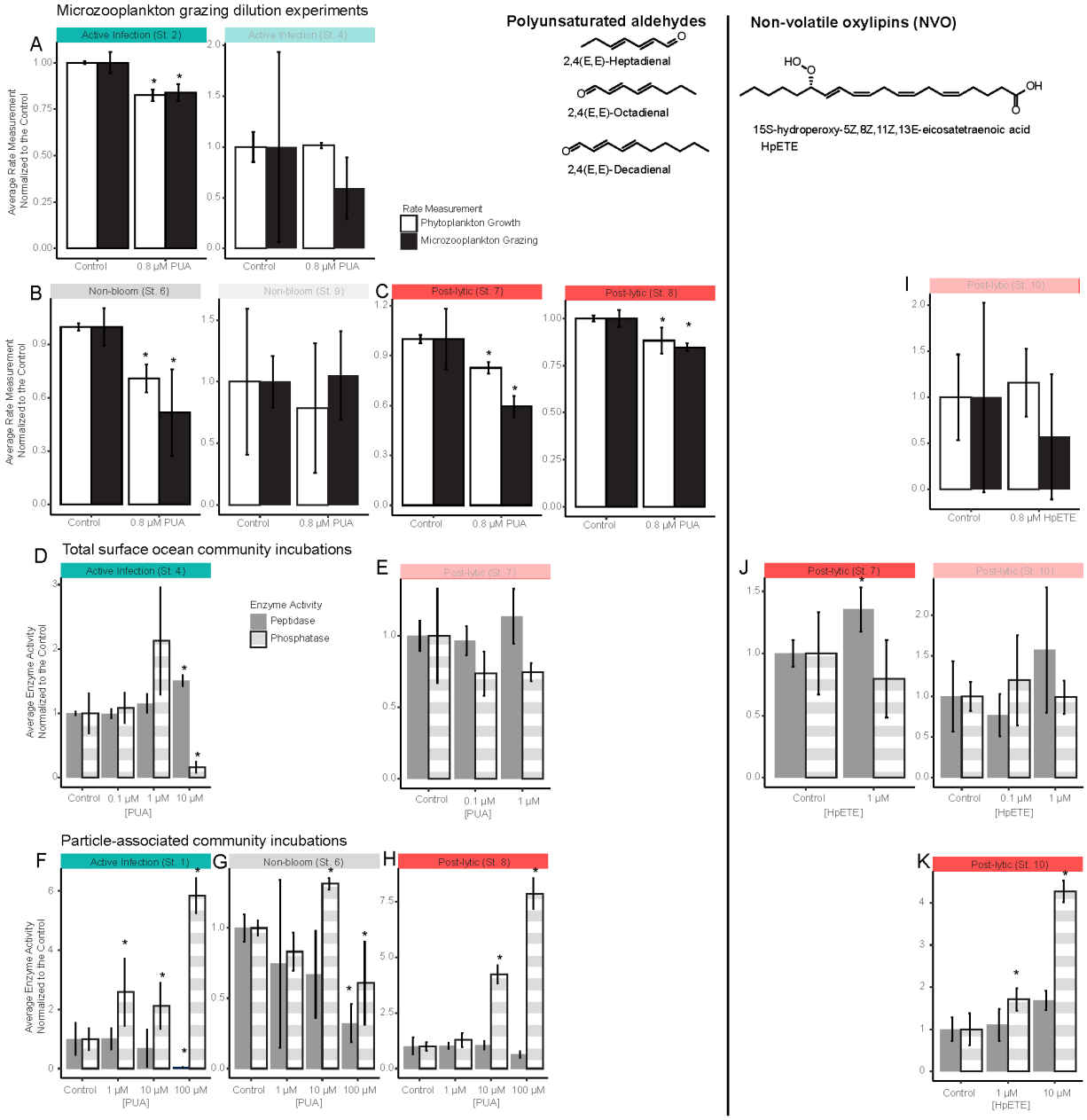

Figure 6. Microzooplankton grazers, phytoplankton, and both the surface and the particle associated heterotrophic microbial communities exhibit dose- and community-dependent responses to specific PUAs and non-volatile oxylipins. A-C, I) Fold-change in growth rate of phytoplankton (white) and grazing rate of microzooplankton (black) for control (untreated) and oxylipin amendments at seven stations. The mean and standard deviation are shown (n=3). Asterisks denote a statistical difference from the control ($p < 0.05$ Mann-Whitney U). Shaded panels denote statistically insignificant results. **D-E, J)** Enzymatic activity of the surface and **F-H, K)** sinking particle-associated microbial communities in response to varying concentrations of a PUA mixture **(D-H)** and the oxylipin 15-hydroxyeicosapentaenoic acid (15-HpETE; **I-K**). Alkaline phosphatase activity is in grey and white stripe and peptidase activity is in solid grey. Values are normalized to the triplicate controls. Asterisks denote a statistically significant difference from the control ($p < 0.1$ Krushal-Wallis with a $p < 0.05$ Dunn's post-hoc).

408 ***Exploring the bioactivity of NVO vs PUAs***
409 As mentioned above, NVOs are thought to be more deleterious to grazers than PUAs. For example,
410 dinoflagellate grazing on diatom cultures is inhibited by 50% at 1 nM NVO but exposure to 10 nM PUA
411 only decreased grazing by 33%; PUA concentrations in the 1000 nM range were needed for a 50%
412 reduction in grazing[33]. To better understand the response to NVOs vs. PUA across multiple trophic levels,
413 a set of grazing-growth experiments (Fig. 6I), two sets of surface microbial enzymatic activity
414 experiments (Fig. 6J), and one set of particle-associated microbial enzymatic activity experiments (Fig.
415 6K) were conducted with the NVO, 15-HpETE, replicating the aforementioned PUA experiment. The
416 grazing experiment with 15-HpETE (Fig. 6I) displayed large variability amongst replicates and a negative
417 growth rate in the control and was inconclusive (Fig. S4D). Enzymatic activity was stimulated by NVOs
418 in both surface and sinking particle-associated microbial communities (Fig. 6J-K). The stimulation of the
419 surface community was more significant for NVOs than PUAs at 1 µM (Fig. 6J *vs.* 6E; St. 7). Similarly,
420 particle-associated community responses to 10 µM PUAs and NVOs additions were observed at the Post-
421 lytic Point Reyes sites (St. 8 and St.10, respectively; Fig. 6H and 6K). We had a limited amount of 15-
422 HpETE stock, so we were restricted to a smaller number of experiments and a limited range of
423 concentrations tested. Additional parallel experiments with NVOs and PUAs are needed to fully
424 understand dose-dependent impacts of oxylipins on the same population. Nonetheless, our results are
425 congruent with studies exploring the effect of various oxylipins on copepods, sea urchins, and
426 dinoflagellate grazing, which suggest that the effective concentration varies by oxylipin[8,10,12,33,65,66].
427
428 Notably, 15-HpETE, the compound tested in deck-board incubations, was observed in the DYEatom
429 cruise meta-lipidome (Fig. S6A). HpETE analogs (*i.e.* compounds annotated as NVO 20:4 +2O at all
430 retention times) were present in significantly higher concentrations at the Post-lytic Point Reyes sites
431 compared to mid infection or non-bloom states (Fig. S6B). HpETE analogs represented less than 1% of
432 the average annotated peak area (Fig. S7). C20:5 and C16:n oxylipins and their free fatty acid precursors
433 dominated the dissolved lipidome representing 58% of the peak area (Fig. S6). Given the dose
434 dependence of oxylipin bioactivity, oxylipin quantification is critical to understanding and contextualizing
435 their bioactivity *in situ*. Our general untargeted approach better captured the wide diversity of compounds
436 present but it only allows for presentation of relative abundances. Future work should take advantage of
437 tractable absolute quantification with an adequate suite of representative authentic standards.
438
439 **Biogeochemical impacts of oxylipin chemical signaling during viral infection**
440 We previously reported enhanced ectoprotease activity at the lytic Point Reyes site, which we interpreted
441 as stimulation of remineralization and the 'viral shunt'[17]. Deck-board experiments in this study revealed
442 oxylipin-inducible enzyme activity in surface and sinking particle-associated microbial communities
443 further connecting virus infection (and the induced chemical signaling) with enhanced organic matter
444 turnover. Silicon dissolution is critically controlled by proteolytic degradation of the organic matrix
445 protecting diatom frustules, denuding and exposing the opal (SiO_2) to the undersaturated seawater[68]. In
446 turn, this dissolved silicic acid ($Si(OH)_4$) can support regenerative biogenic silica production[69]. Enhanced
447 silica dissolution can also negatively impact mineral ballasting of exported carbon and diminish the
448 oceanic silica pump[70]. We conducted experiments to test whether oxylipin enhanced enzymatic activity
449 impacted biogenic silica dissolution, but it was inconclusive (data not presented). The stimulation of
450 ectopeptidase in surface microbial communities has been observed in diatom blooms in this region[70]. The
451 mechanisms underlying peptidase stimulation during viral infection of *Chaetoceros*[20] are not well

understood but could be linked to the production of nitrogen-rich, Coomassie Stainable Particles (CSP), which have been observed in virus-infected *Chaetoceros* culture studies[71]. Stimulation of peptidase over phosphatase in the surface ocean would serve to preferentially remineralize nitrogen from dissolved organic matter and is consistent with nitrogen being the co-limiting nutrient in the sunlit CCE along with Fe rather than phosphorus[72]. A preference for phosphatase stimulation on particles reflects a shift in community activity towards accessing organically bound phosphate in response to oxylipin chemical signaling below the euphotic zone.

At the same time, our geochemical data (Fig. 4A-C) strongly suggest that virus infection of this natural diatom community induced the viral shuttle and enhanced carbon export even with enhanced enzymatic turnover of organic material in surface communites[17]. Export was positively correlated with the total peak intensity of oxylipins in the dissolved lipidome (Fig. S5A), suggesting that oxylipins may play a role in enhanced export during infection. The relative balance between shunt versus shuttle outcomes will ultimately be determined by the remineralization length scales relative to the mixed layer depth (see Figure 5 in Kranzler et al.[20]). In our study, virus infection stimulated export flux and high e-ratios to 50 m; the observed MLD at this station was 10 m, thus driving the net outcome towards the shuttle.

Evidence of a strong viral shuttle was previously observed in coccolithophores populations that were actively infected with giant, double-stranded DNA-containing Coccolithoviruses in the North Atlantic[59]; diagnostic lipid biomarkers[48,73,74] showed that sinking aggregates were enriched with infected cells and resulted in very high POC and PIC fluxes. Similarly, eukaryotic viral marker genes in a meta'omic study of the TARA Oceans Expedition global dataset explained 67% of the variability in carbon export efficiency with 58 viruses positively correlated and 25 negatively correlated with export efficiency[19]. Many of the positively correlated viruses were linked to silicifying eukaryotes, like diatoms. Mechanistically, culture studies with eukaryotic phytoplankton, including diatoms and coccolithophores, have shown that virus infection enhances spore formation[75], TEP and CSP excretion, and particle aggregation [71,76]. Oxylipins are known to increase aggregation in the benthic diatom *Fistulifera saprophila*[77] but these effects are strain dependent.

In addition to remineralization length scales of sinking particles, population dynamics have been proposed as important controls on whether viral infection leads to enhanced export or upper ocean recycling. Large scale mesocosm experiments show a 2-4x increase in TEP and PIC production per cell for *G. huxleyi* during infection feeding into the viral shuttle and resulting in adsorption of viruses from the water column on to aggregated particles. Taken with the data presented here and the conceptualization of larger phytoplankton being associated with more zooplankton degradation and higher overall fluxes, we hypothesize that eukaryotic algae are more subject to the viral shuttle compared to prokaryotic hosts. The remineralization length scale plays into this as eukaryotic phytoplankton sink faster than prokaryotes as a function of size and added density due to associated biominerals; thus, the length scale over which their biomass can be remineralized is longer leading to more efficient carbon export. Our analysis adds a layer of complexity to the dynamic controls on viral carbon cycling with oxylipin-producing diatom populations altering organic matter recycling, grazing, growth, and export. The dose dependent nature of oxylipin signaling may contribute to episodic export once inhibitory thresholds for the community are surpassed, resulting in a toggle between shuttle and shunt (Fig. 7).

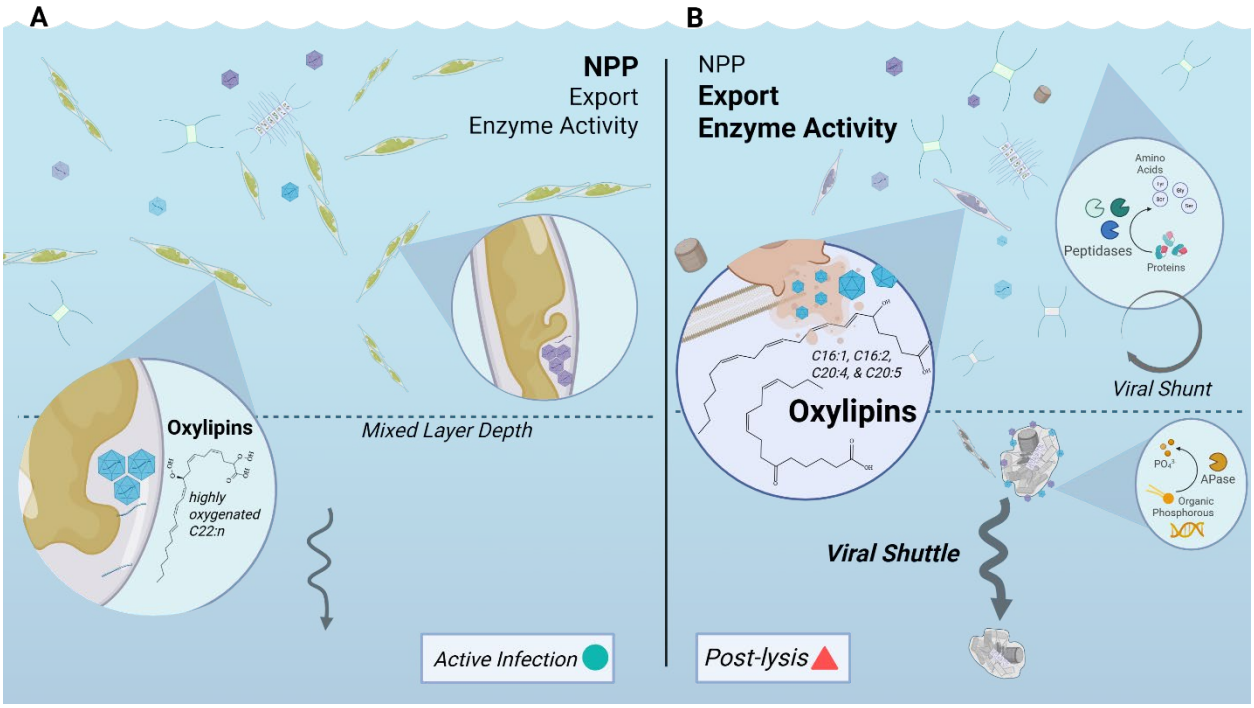

Figure 7. Oxylipin chemical signaling during virus infection and bloom demise toggles the fate of organic matter between export and remineralization. Conceptual link between the state of virus infection, oxylipin production, export flux, and remineralization length scale in a natural diatom population. **A)** Communities undergoing active infection (such as those surveyed near Monterey Bay on June 28th) were at the peak bloom NPP, as per satellite measurements and *in situ* chlorophyll accumulation. Some oxylipins are detected in the environment but at lower levels and were characterized by a different suite of compounds. **B)** Lytic populations (such as those surveyed at Point Reyes) had higher dissolved oxylipin concentrations, including those specifically viral biomarkers from culture infection studies, along with decreases in NPP over the proceeding 8 d, higher export flux and e-ratios of carbon to 50 m (compared to Monterey Bay), and higher ectoenzymatic activities. Taken together, these data suggest that virus infection and oxylipins induced the viral shuttle and enhanced carbon export even with enhanced turnover of organic matter remineralization indicative of the viral shunt[17]. The dashed horizontal line in each panel represents the mixed layer depth.

Conclusions

Several, specific oxylipins were identified as biomarkers for viral infection and cell mortality in cultured *Chaetoceros* sp. and were subsequently found in the meta-lipidomes of virus-infected natural diatom communities infected in the California Current Ecosystem. Deck-board incubations agreed with microbial responses to oxylipin observed in previous studies, namely dose-, compound-, and community-dependent inhibition of grazing and phytoplankton growth and stimulation of particle-associated microbial communities. Oxylipins stimulated phosphatase activity on sinking particles and peptidase activity in surface communities, while inhibiting microzooplankton grazing and phytoplankton growth. Biogeochemical measurements suggest that virus-mediated diatom bloom decline led to higher and more efficient carbon export compared to earlier phases of infection, despite stimulatory effects on enzymatic remineralization of organic matter. Taken together, these findings highlight how viruses and chemical signaling via oxylipins mediate trophic interactions and biogeochemical fate of organic matter in productive upwelling regimes.

Materials and Methods

Viral Infection Experiments with Cultured Chaetoceros sp.

Cultures of the diatom hosts *C. socialis* strain NIES-3713 (formerly L-4) and *C. tenuissimus* strains NIES-3714 (formerly 2-6) and NIES-3715 (formerly 2-10) were grown in SWM-3 media at 15°C under 150 µmols photons m^{-2} s^{-1} irradiance on a 12:12 L:D photoperiod. Triplicate cultures were infected during exponential growth with CsfrRNAV (*C. socialis*), CtenRNAV (*C. tenuissimus* NIES-3715) or CtenDNAV (*C. tenuissimus* NIES-3715). Samples were collected for cell counts via microscopy or flow cytometry. For experiments with CsfrRNAV and CtenRNAV, samples for dissolved lipidome analysis were collected at 0, 1, and 3 dpi, representing early, mid, and late infection, respectively (Fig. S2). For experiments with CtenDNAV, samples for dissolved lipidome analysis were collected 0, 1, 3, and 4 dpi. Triplicate uninfected control cultures were sampled concurrently to exclude changes during normal growth. Follow-up experiments grew the two hosts, along with *C. tenuissimus* NIES-3714 into decline phase to assess changes associated with death (likely induced by nutrient limitation). Samples were pre-filtered through a 0.2 µM Durapore filter to remove particles. The deuterated internal standard, 15(S)-Hydroxy eicosatetraenoic acid-d8 (Cayman Chemical), was added to each filtered sample to a final concentration of 10 µM. The dissolved lipids were then extracted onto a Waters HLB SPE cartridge.

Lipidomic Analysis

The dissolved lipids were eluted from the SPE cartridge with 2 ml of 70:30 acetonitrile: isopropanol into pre-combusted collection vials that were treated with the antioxidant BHT to prevent autoxidation of the samples. The samples were immediately transferred from the collection vials into HPLC vials and capped under argon. The samples were stored at -80°C until mass spectrometric analysis. Within a week of extraction the dissolved lipidome samples were analyzed using reverse phase HPLC (Agilent 1200 system; Agilent, Santa Clara, CA, USA) paired with high resolution, accurate mass (HRAM) data from a Thermo Exactive Plus Orbitrap mass spectrometer (ThermoFisher Scientific, Waltham, MA, USA). The chromatographic method used a Xbridge C8 column (Waters, Milford, MA, USA) as the stationary phase, 18 MΩ water as eluent A, 70:30 acetonitrile: isopropanol as eluent B, and ammonium acetate and acetic acid as the adduct forming additives[70]. The gradient began with a 1-minute isocratic hold of 45% B and shifted to 99% B over 25 minutes with a flow rate of 0.4 mL min^{-1}. Full scan data (m/z 100-1500) was collected in negative mode at a mass resolution of 170,000. For the follow-up experiments and to annotate the oxylipins in the original Chaetoceros and DYEatom cruise samples, the dissolved lipid extracts were analyzing using reverse phase chromatography (Vanquish UHPLC, ThermoFisher Scientific, San Jose, CA, USA) paired with HRAM data-dependent acquisition on a Orbitrap ID-X mass spectrometry (ThermoFisher Scientific, San Jose, CA, USA). A mass inclusion list with the exact masses of $[M-H]^-$ adducts of important oxylipins was used to acquire ms^2 for further annotation (*Chaetoceros* experiment oxylipin annotation described in Edwards et al. 2024; DYEatom annotation in Table S5). For further details, please refer to the manuscript detailing the intercomparison of diatom host-virus pairs[16].

Chemoinformatic Pipeline

The raw mass spectrometric data was converted to mzXML format with mscovert and analyzed with the R packages xcms[78–80] and CAMERA[81], which aligned the chromatograms, picked and integrated peaks, and identified and removed secondary isotopic peaks (specific details in Edwards *et al*., 2024). The lipidomic features were further annotated using the LOBSTAHS package which included m/z information

of the various acyl chain-lengths, degrees of unsaturation, and oxidations of triacylglycerols, free fatty acids (FFA), polyunsaturated aldehydes (PUA), and eight intact polar diacylglycerol lipids and their most common adducts[82]. The features annotated as oxylipins, and free fatty acids were retained and manually verified as high-quality peaks in El-MAVEN[83–85]. The fragmentation of the compounds was assessed using the rerun of the 2016 samples on the UPLC-Orbitrap ID-X and in silico databases created by the Edwards Lab in CFM-ID[86], and iterative database of mammalian oxylipins from Watrouse[87], and the *in silico* database of algae, plant, and animal lipids available through the LipidBlast pathway in MS-DIAL[88]. Peak areas were normalized to the recovery of the internal standard and volume filtered. Statistical analyses were performed using the R package MetaboAnalyst through its web interface[54].

DYEatom cruise

The DYEatom cruise aboard the R/V Point Sur (PS1312) disembarked from Moss Landing, CA on June 27, 2013. The 9-day cruise track transected the California coastal upwelling region (Fig 4 and Table S4). Nine stations were occupied. The details of the metatranscriptomic analysis of cell associated viruses and qPCR of free-living viruses used for assessing viral infection by diatom RNA viruses can be found in Kranzler *et al.* 2019, where the details of the enzyme activity protocols can also be found[17].

Dissolved Meta-lipidome

The dissolved lipidome was sampled at two depths in the water column along the cruise track, the 55% Io depth and the chlorophyll maximum. One liter of seawater from each depth was filtered through a bottle top 0.2 µm filter (Corning) to remove particulate material. The internal standard benzaldehyde (Sigma-Aldrich) was added to a final concentration of 10 µM in one liter of seawater. Using a vacuum manifold, the samples were filtered onto a Water HLB solid phase extraction (SPE) cartridge for approximately one hour and the final volume filtered was recorded. The SPE cartridges were acidified with 0.1% hydrochloric acid, placed in a whirl-pak bag, and stored at -80°C until elution and analysis at Woods Hole Oceanographic Institution. Samples were analyzed using the chromatographic, mass spec, and lipidomic pipeline outlined above.

Sediment Trap Collection of Sinking Particles

At Stations 1, 6, 8, and 10, sinking particles were collected using a surface tethered net trap deployed at a depth of 50m for ~8 hrs. Trap material was screened through a 350 µm mesh to exclude larger mesozooplankton and split into 8 equal 500 mL fractions using a rotating electric splitter[89,90]. One 500-mL split of the trap material was filtered onto three pre-combusted 47mm glass fiber filters (nominal pore size- 0.7-µm) for particulate organic carbon and nitrogen (POC/PON) analysis. The samples were kept at −80 °C until analysis at Woods Hole Oceanographic Institution (Woods Hole, MA) on a Finnigan- MAT DeltaPlus stable light isotope ratio mass spectrometer[91]. The POC and PON values of the three filters were summed together for each trap and deployment time was used to calculate flux to 50 m over a 24-hour period.

Net Primary Productivity Estimates

High-resolution, 8-day integrated satellite-based estimates of net primary productivity in the CCE for the month surrounding our cruise were downloaded from the Oregon State University Ocean Productivity website. The NPP estimates come from the CAFE model, which is depth, time, and spectrally resolved[55]. Clara Douglas wrote the MatLab script for this analysis.

611
612 ***Deck-board Incubations***
613 Three types of amendment experiments were conducted at sea: 1) three deck-board incubation
614 experiments with surface seawater communities and varying concentrations, of either a mix of PUAs (0,
615 0.1, and 1μM) or the NVO, 15-HpETE (0 , 0.1, and 1 μM; Fig. 6B), 2) four dark incubation experiment
616 with sinking particles from 50 m amended with 0 , 1, and 10 μM HpETE or 0, 1, 10, and 100 μM PUA
617 (Fig. 6C); 3) seven deck-board paired dilution experiments to compare microzooplankton grazing rates
618 and phytoplankton growth rate in no amendment controls and 1 μM PUA or 0.8 μM HpETE treatments
619 (Fig. 6A). These concentrations were chosen based on the bioactive PUA concentrations for marine
620 bacterial isolates[28], PUA concentrations that enhanced the metabolism of marine microbes associated with
621 sinking particles in the North Atlantic[35], and PUA concentrations that decreased microzooplankton
622 growth rate in the Chesapeake Bay[32].
623
624 *Stock solutions*
625 The NVO 15-HpETE stock solution was biosynthesized in the lab by adding the enzyme 15-lipoxygenase
626 (Sigma-Aldrich) to arachidonic acid (Sigma-Aldrich) using the protocol outlined in Iacazio *et al.* (1990)[92].
627 Once the reaction reached completion, the oxylipins were extracted onto an SPE cartridge (HBL Waters)
628 and immediately eluted with methanol. Mass spectrometric analysis determined the composition of the
629 oxylipin stock was 825 mmol L^{-1} 15-HpETE and a background of its precursor and positional isomers.
630 The oxylipin stock solution was capped under N_2 and stored at -20 °C. In our LOBSTAHs notation
631 HpETE is FFA 20:4 +2O.
632
633 A stock solution containing a mix of polyunsaturated aldehydes was prepared at sea and contained 100
634 mM of 2,4-heptdienal, 2.4-octadienal, and 2,4- decadienal (Sigma-Aldrich) dissolved in methanol. The
635 solution was kept at 4C and was remade every two days to prevent degradation. In our LOBSTAHS
636 notation these compounds would be PUA 7:2, PUA 8:2 and PUA 10:2.
637
638 *Surface Ocean Community*
639 At Stations 4, 7, and 10, seawater was collected from the 55% I_0 depth into 2 L Nalgene bottles. At St. 4,
640 0, 0.1, 1 and 10 μM PUAs were added to triplicate bottles using methanol as a carrier liquid. Care was
641 taken such that the same volume of methanol was added to each treatment including the 0 μM control. At
642 St. 7, 0, 0.1, and1 μM PUA and 1 μM HpETE were added to bottles in triplicate. At St. 10, we began to
643 run out of oxylipin stocks so only three conditions were made up in triplicate: 0, 0.1, and 1 μM HpETE.
644 The 2 L microcosms were placed in on-deck incubators screened to mimic the light field at 55% I_0 and
645 temperature controlled by a flow through system for ~24 hours. Enzymatic activity was measured at the
646 end of the experiment (Fig. 6B) using fluorogenic substrates as described in Kranzler *et al.* 2019[17].
647
648 *Particle Associated Community*
649 At the stations where sinking particles were collected, a 500 mL split was used to set up dark incubations
650 using the experimental design laid out in Edwards et al 2015. In a dark on-deck incubator that was
651 temperature controlled by a flow-through system, the trap material was incubated in opaque 150 mL
652 Nalgene bottles in triplicate for 24 hours. At St 1, 6, and 8, the treatments were 0, 1, 10, and 100 μM
653 PUA. At St. 10, the treatment was 0, 1, or 10 μM HpETE Enzymatic activity was measured at the end of
654 each experiment (Fig. 6C). Samples were also taken for biogenic silica quantification by filtering 25 mL

onto a 1.2 µm nucleopore filter for analysis at Rutgers (Fig. S8A). The same volume was filtered through a 0.7 µm nucleopore and frozen for dissolved Si analysis at UCSB (Fig. S8B).

Grazing and Growth Rate- Dilution Experiments

Paired dilution experiments were conducted to measure microzooplankton grazing rates and phytoplankton growth rates with and without exposure to exogenous oxylipins, at seven stations along the cruise track (Fig. 6A and S4). At each station, 40 L of water was collected from the depth of 50% surface photosynthetically active radiation (PAR). Half of this volume was then gravity filtered through a 200 µm Nitex mesh, to be used as whole seawater (WSW), and stored in an on-deck incubator at *in situ* surface temperature until the experimental set-up. The other 20 L was gravity filtered through a 20 µm Nitex mesh, to gently remove large phytoplankton (i.e. diatoms), and then gravity filtered through a Pall 0.2 µm vented sterile filter capsule, in order to make dilution water. Once the dilution water was prepared, we used a modified dilution method[93] with three points, using 5, 20, and 100% WSW, in triplicate 1L bottles. Nutrients were not added to bottles. For treated bottles, a final concentration of 0.8 µM oxylipins were added using a stock solution prepared in the lab. All dilution bottles were sampled at time 0 and after 20-24h for chlorophyll, cell counts (1% gluteraldehyde), and FIRe analysis, while only 100% WSW bottles were sampled at both time points for microzooplankton abundance (10% Lugol's).

Statistical analyses for incubation experiments

For the oxylipin amendment experiments, Shapiro-Wilk tests showed that the data was not normally distributed and non-parametric rank-order tests were used to determine significant differences between treatments (Sigma-Plot). A Mann-Whitney U was utilized to test whether microzooplankton grazing rate and the phytoplankton growth rates from the paired dilution experiments were significantly different in the no amendment controls compared to the 0.8 µM HpETE treatments. A Kruskal-Wallis analysis of variance on ranks was used to determine if the enzymatic activity of peptidase and phosphatase was significantly different in the controls compared to the oxylipin treatments in amendment experiments, as well as, to determine if the total peak area of annotated free fatty acids and oxylipins was significantly different between the significant groups of samples revealed by similarity profile analysis ($p < 0.1$). Dunn's method was used as a post-hoc to determine which groups were different from one another ($p < 0.05$).

Data Accessibility

The dissolved lipidomes are available on the MassIVE repository. Biogeochemical data from the DYEatom cruise can be found on BCO-DMO (PS1312, http://www.bco-dmo.org/project/550825).

Acknowledgements

The captain and crew of the *R/V Pt. Sur* and the Brzezinski lab group who also sailed with us. We thank Yuji Tomaru (Fisheries Technology Institute, Japan Fisheries Research and Education Agency) for providing the *Chaetoceros* diatom host-virus systems. We thank the funding sources that supported this work: NSF OCE-1155663 (to JWK), Gordon and Betty Moore Foundation (BVM, KDB, MJ), McMinn Endowed Fund (BRE), NSF OCE- (BRE),

1. Leblanc, K. *et al. Distribution of Calcifying and Silicifying Phytoplankton in Relation to Environmental and Biogeochemical Parameters during the Late Stages of the 2005 North*

East Atlantic Spring Bloom. *Biogeosciences* vol. 6 www.biogeosciences.net/6/2155/2009/ (2009).

2. Behrenfeld, M. J., Boss, E. S. & Halsey, K. H. Phytoplankton community structuring and succession in a competition-neutral resource landscape. *ISME Communications* **1**, (2021).
3. Jin., X., Gruber, N., Dune, J. P., Sarmiento, J. L. & Armstrong, R. A. Diagnosing the contributions of phytoplankton functional groups to the production and export of particulate organic carbon, CaCO3, and opal from global nutrient and alkalinity distributions. *Global Biogeochem Cycles* **20**, (2006).
4. Benoiston, A. S. *et al.* The evolution of diatoms and their biogeochemical functions. *Philosophical Transactions of the Royal Society B: Biological Sciences* vol. 372 Preprint at https://doi.org/10.1098/rstb.2016.0397 (2017).
5. Bianchi, T. S. *et al.* Centers of organic carbon burial and oxidation at the land-ocean interface. *Organic Geochemistry* vol. 115 138–155 Preprint at https://doi.org/10.1016/j.orggeochem.2017.09.008 (2018).
6. Miralto, A. *et al.* The insidious effect of diatoms on copepod reproduction. *Nature* **402**, 173–176 (1999).
7. Ianora, A. *et al.* Aldehyde suppression of copepod recruitment in blooms of a ubiquitous planktonic diatom. *Nature* **429**, 403–407 (2004).
8. Ianora, A. *et al.* Non-volatile oxylipins can render some diatom blooms more toxic for copepod reproduction. *Harmful Algae* **44**, 1–7 (2015).
9. Brugnano, C. *et al.* The deleterious effect of diatoms on the biomass and growth of early stages of their copepod grazers. *J Exp Mar Biol Ecol* **476**, 41–49 (2016).
10. Lauritano, C. *et al.* New oxylipins produced at the end of a diatom bloom and their effects on copepod reproductive success and gene expression levels. *Harmful Algae* **55**, 221–229 (2016).
11. Turner, J. T., Ianora, A., Miralto, A., Laabir, M. & Esposito, F. Decoupling of copepod grazing rates, fecundity and egg-hatching success on mixed and alternating diatom and dinoflagellate diets. *Mar Ecol Prog Ser* **220**, 187–199 (2001).
12. Ianora, A. *et al.* Low reproductive success for copepods during a bloom of the non-aldehyde-producing diatom Cerataulina pelagica in the North Adriatic Sea. *Marine Ecology* **29**, 399–410 (2008).
13. Barreiro Felpeto, A. *et al.* Diatom induction of reproductive failure in copepod: The effect of PUAs versus non volatile oxylipins. *J Exp Mar Biol Ecol* **401**, 13–19 (2011).
14. Ribalet, F. *et al.* Age and nutrient limitation enhance polyunsaturated aldehyde production in marine diatoms. *Phytochemistry* **68**, 2059–2067 (2007).
15. Ribalet, F. *et al.* High Plasticity in the Production of Diatom-derived Polyunsaturated Aldehydes under Nutrient Limitation: Physiological and Ecological Implications. *Protist* **160**, 444–451 (2009).
16. Edwards, B. R., Thamatrakoln, K., Fredricks, H. F., Bidle, K. D. & Van Mooy, B. A. S. Viral Infection Leads to a Unique Suite of Allelopathic Chemical Signals in Three Diatom Host–Virus Pairs. *Mar Drugs* **22**, (2024).
17. Kranzler, C. F. *et al.* Silicon limitation facilitates virus infection and mortality of marine diatoms. *Nat Microbiol* (2019) doi:10.1038/s41564-019-0502-x.

18. Vincent, F. *et al.* Viral infection switches the balance between bacterial and eukaryotic recyclers of organic matter during coccolithophore blooms. *Nat Commun* **14**, (2023).
19. Kaneko, H. *et al.* Eukaryotic virus composition can predict the efficiency of carbon export in the global ocean. *iScience* **24**, (2021).
20. Kranzler, C. F. *et al. Taxonomically Distinct Diatom Viruses Differentially Impact Microbial Processing of Organic Matter*. *Sci. Adv* vol. 11 https://www.science.org (2025).
21. Jagusch, H., Baumeister, T. U. H. & Pohnert, G. Mammalian-Like Inflammatory and Pro-Resolving Oxylipins in Marine Algae. *ChemBioChem* **21**, 2419–2424 (2020).
22. Wichard, T. *et al.* Survey of the Chemical Defence Potential of Diatoms: Screening of Fifty Species for α,β,γ,δ-unsaturated aldehydes. *J Chem Ecol* **31**, 949–958 (2005).
23. Ribalet, F. *et al.* Phytoplankton cell lysis associated with polyunsaturated aldehyde release in the Northern Adriatic Sea. *PLoS One* **9**, e85947–e85947 (2014).
24. Gerecht, A. *et al.* Oxylipin production during a mesocosm bloom of Skeletonema marinoi. *J Exp Mar Biol Ecol* **446**, 159–165 (2013).
25. Russo, E. *et al.* Density-dependent oxylipin production in natural diatom communities: possible implications for plankton dynamics. *ISME J* **14**, 164–177 (2020).
26. Barbarinaldi, R. *et al.* Prostaglandin pathway activation in the diatom Skeletonema marinoi under grazer pressure. *Mar Environ Res* **196**, (2024).
27. Ribalet, F., Berges, J. A., Ianora, A. & Casotti, R. Growth inhibition of cultured marine phytoplankton by toxic algal-derived polyunsaturated aldehydes. *Aquatic Toxicology* **85**, 219–227 (2007).
28. Ribalet, F., Intertaglia, L., Lebaron, P. & Casotti, R. Differential effect of three polyunsaturated aldehydes on marine bacterial isolates. *Aquat Toxicol* **86**, 249–255 (2008).
29. Vardi, A. *et al.* A Stress Surveillance System Based on Calcium and Nitric Oxide in Marine Diatoms. *PLoS Biol* **4**, e60- (2006).
30. Pepi, M. *et al.* Toxicity of diatom polyunsaturated aldehydes to marine bacterial isolates reveals their mode of action. *Chemosphere* **177**, 258–265 (2017).
31. Franzè, G., Pierson, J. J., Stoecker, D. K. & Lavrentyev, P. J. Diatom-produced allelochemicals trigger trophic cascades in the planktonic food web. *Limnol Oceanogr* **63**, 1093–1108 (2018).
32. Lavrentyev, P. J., Franzè, G., Pierson, J. J. & Stoecker, D. K. The effect of dissolved polyunsaturated aldehydes on microzooplankton growth rates in the Chesapeake Bay and Atlantic coastal waters. *Mar Drugs* **13**, 2834–2856 (2015).
33. Johnson, M. D., Edwards, B. R., Beaudoin, D. J., Van Mooy, B. A. S. & Vardi, A. Nitric oxide mediates oxylipin production and grazing defense in diatoms. *Environ Microbiol* **22**, 629–645 (2020).
34. Wu, Z., Li, Q. P., Ge, Z., Huang, B. & Dong, C. Impacts of biogenic polyunsaturated aldehydes on metabolism and community composition of particle-attached bacteria in coastal hypoxia. *Biogeosciences* **18**, 1049–1065 (2021).
35. Edwards, B. R., Bidle, K. D. & Van Mooy, B. A. S. Dose-dependent regulation of microbial activity on sinking particles by polyunsaturated aldehydes: Implications for the carbon cycle. *Proc Natl Acad Sci U S A* **112**, 5909–5914 (2015).

36. Ianora, A. & Miralto, A. Toxigenic effects of diatoms on grazers, phytoplankton and other microbes: A review. *Ecotoxicology* **19**, 493–511 (2010).
37. Stoecker, D. K. *et al.* Underestimation of microzooplankton grazing in dilution experiments due to inhibition of phytoplankton growth. *Limnol Oceanogr* **60**, 1426–1438 (2015).
38. Vidoudez, C., Casotti, R., Bastianini, M. & Pohnert, G. Quantification of dissolved and particulate polyunsaturated aldehydes in the Adriatic Sea. *Mar Drugs* **9**, 500–503 (2011).
39. Wu, Z., Li, Q. P., Dong, Y., Xu, J. & Luo, L. High-Resolution Surveys of Phytoplankton-Derived Polyunsaturated Aldehydes at Frontal Zones Outside a Eutrophic Estuary. *J Geophys Res Biogeosci* **126**, e2020JG005808 (2021).
40. Wu, Z., Li, Q. P., Ge, Z., Huang, B. & Dong, C. Impacts of biogenic polyunsaturated aldehydes on metabolism and community composition of particle-Attached bacteria in coastal hypoxia. *Biogeosciences* **18**, 1049–1065 (2021).
41. Stoecker, D. K. *et al.* Underestimation of microzooplankton grazing in dilution experiments due to inhibition of phytoplankton growth. *Limnol Oceanogr* **60**, 1426–1438 (2015).
42. Kolody, B. C. *et al.* Diel transcriptional response of a California Current plankton microbiome to light, low iron, and enduring viral infection. *ISME J* **13**, 2817–2833 (2019).
43. Krause, J. W. *et al.* The interaction of physical and biological factors drives phytoplankton spatial distribution in the northern California Current. *Limnol Oceanogr* **65**, 1974–1989 (2020).
44. Bolaños, L. M. *et al.* Small phytoplankton dominate western North Atlantic biomass. *ISME Journal* **14**, 1663–1674 (2020).
45. de Vargas, C. *et al. Eukaryotic Plankton Diversity in the Sunlit Ocean*. *Stefanie Kandels-Lewis* vol. 15 https://www.science.org.
46. Mojica, K. D. A., Huisman, J., Wilhelm, S. W. & Brussaard, C. P. D. Latitudinal variation in virus-induced mortality of phytoplankton across the North Atlantic Ocean. *ISME J* **10**, 500–513 (2016).
47. Eich, C. *et al.* Ecological Importance of Viral Lysis as a Loss Factor of Phytoplankton in the Amundsen Sea. *Microorganisms* **10**, (2022).
48. Vardi, A. *et al.* Viral glycosphingolipids induce lytic infection and cell death in marine phytoplankton. *Science (1979)* **326**, 861–865 (2009).
49. Diaz, B. P. *et al.* Seasonal mixed layer depth shapes phytoplankton physiology, viral production, and accumulation in the North Atlantic. *Nat Commun* **12**, 6634 (2021).
50. Kimura, K. & Tomaru, Y. Isolation and Characterization of a Single-Stranded DNA Virus Infecting the Marine Diatom Chaetoceros sp. Strain SS628-11 Isolated from Western JAPAN. *PLoS One* **8**, e82013- (2013).
51. Tomaru, Y., Takao, Y., Suzuki, H., Nagumo, T. & Nagasaki, K. Isolation and Characterization of a Single-Stranded RNA Virus Infecting the Bloom-Forming Diatom Chaetoceros socialis *Appl Environ Microbiol* **75**, 2375 (2009).
52. Tomaru, Y. *et al.* Isolation and characterization of a single-stranded RNA virus that infects the marine planktonic diatom Chaetoceros sp. (SS08-C03). *Phycological Res* **61**, 27–36 (2013).

53. Pang, Z. *et al.* Using MetaboAnalyst 5.0 for LC–HRMS spectra processing, multi-omics integration and covariate adjustment of global metabolomics data. *Nat Protoc* **17**, 1735–1761 (2022).
54. Chong, J., Wishart, D. S. & Xia, J. Using MetaboAnalyst 4.0 for Comprehensive and Integrative Metabolomics Data Analysis. *Curr Protoc Bioinformatics* **68**, e86 (2019).
55. Silsbe, G. M., Behrenfeld, M. J., Halsey, K. H., Milligan, A. J. & Westberry, T. K. The CAFE model: A net production model for global ocean phytoplankton. *Global Biogeochem Cycles* **30**, 1756–1777 (2016).
56. Boeuf, D. *et al.* Biological composition and microbial dynamics of sinking particulate organic matter at abyssal depths in the oligotrophic open ocean. *Proc Natl Acad Sci U S A* **116**, 11824–11832 (2019).
57. Luo, E., Leu, A. O., Eppley, J. M., Karl, D. M. & DeLong, E. F. Diversity and origins of bacterial and archaeal viruses on sinking particles reaching the abyssal ocean. *ISME Journal* **16**, 1627–1635 (2022).
58. Karl, D. M., Church, M. J., Dore, J. E., Letelier, R. M. & Mahaffey, C. Predictable and efficient carbon sequestration in the North Pacific Ocean supported by symbiotic nitrogen fixation. *Proc Natl Acad Sci U S A* **109**, 1842–1849 (2012).
59. Laber, C. P. *et al.* Coccolithovirus facilitation of carbon export in the North Atlantic. *Nat Microbiol* **3**, 537–547 (2018).
60. Mojica, K. D. A. & Brussaard, C. P. D. Factors affecting virus dynamics and microbial host–virus interactions in marine environments. *FEMS Microbiol Ecol* **89**, 495–515 (2014).
61. Buesseler, K. O. *et al.* An assessment of the use of sediment traps for estimating upper ocean particle fluxes. *Journal of Marine Research* vol. 65 345–416 Preprint at https://doi.org/10.1357/002224007781567621 (2007).
62. Siegel, D. A., Devries, T., Cetini´c, I. C. & Bisson, K. M. Quantifying the Ocean's Biological Pump and Its Carbon Cycle Impacts on Global Scales. *Downloaded from www.annualreviews.org. Guest* (2023) doi:10.1146/annurev-marine-040722.
63. Henson, S. A. *et al.* A reduced estimate of the strength of the ocean's biological carbon pump. *Geophys Res Lett* **38**, (2011).
64. Nanjappa, D., d'Ippolito, G., Gallo, C., Zingone, A. & Fontana, A. Oxylipin diversity in the diatom family Leptocylindraceae reveals DHA derivatives in marine diatoms. *Mar Drugs* **12**, 368–384 (2014).
65. Esposito, R. *et al.* Combined Effects of Diatom-Derived Oxylipins on the Sea Urchin Paracentrotus lividus. *Int J Mol Sci* **21**, 719 (2020).
66. Balestra, C., Alonso-Sáez, L., Gasol, J. M. & Casotti, R. Group-specific effects on coastal bacterioplankton of polyunsaturated aldehydes produced by diatoms. *Aquatic Microbial Ecology* **63**, 123–131 (2011).
67. Paul, C. *et al.* Diatom derived polyunsaturated aldehydes do not structure the planktonic microbial community in a mesocosm study. *Mar Drugs* **10**, 775–792 (2012).
68. Bidle, K. D. & Azam, F. Accelerated dissolution of diatom silica by marine bacterial assemblages. *Nature* **397**, 508–512 (1999).

69. Brzezinski, M. A., Jones, J. L., Bidle, K. D. & Azam, F. The balance between silica production and silica dissolution in the sea: Insights from Monterey Bay, California, applied to the global data set. *Limnol Oceanogr* **48**, 1846–1854 (2003).
70. Bidle, K. D., Brzezinski, M. A., Long, R. A., Jones, J. L. & Azam, F. Diminished efficiency in the oceanic silica pump caused by bacteria-mediated silica dissolution. *Limnol Oceanogr* **48**, 1855–1868 (2003).
71. Yamada, Y., Tomaru, Y., Fukuda, H. & Nagata, T. Aggregate formation during the viral lysis of a marine diatom. *Front Mar Sci* **5**, (2018).
72. Deutsch, C. *et al.* Biogeochemical variability in the California Current System. *Prog Oceanogr* **196**, (2021).
73. Hunter, J. E., Frada, M. J., Fredricks, H. F., Vardi, A. & Van Mooy, B. A. S. Targeted and untargeted lipidomics of Emiliania huxleyi viral infection and life cycle phases highlights molecular biomarkers of infection, susceptibility, and ploidy. *Front Mar Sci* **2**, (2015).
74. Vardi, A. *et al.* Host–virus dynamics and subcellular controls of cell fate in a natural coccolithophore population. *Proceedings of the National Academy of Sciences* **109**, 19327–19332 (2012).
75. Pelusi, A. *et al.* Virus-induced spore formation as a defense mechanism in marine diatoms. *New Phytologist* **229**, 2251–2259 (2021).
76. Nissimov, J. I. *et al.* Dynamics of transparent exopolymer particle production and aggregation during viral infection of the coccolithophore, Emiliania huxleyi. *Environ Microbiol* **20**, 2880–2897 (2018).
77. Leflaive, J. & Ten-Hage, L. Effects of 2E,4E-Decadienal on Motility and Aggregation of Diatoms and on Biofilm Formation. *Microb Ecol* **61**, 363–373 (2011).
78. Smith, C. A., Want, E. J., O'Maille, G., Abagyan, R. & Siuzdak, G. XCMS: Processing mass spectrometry data for metabolite profiling using nonlinear peak alignment, matching, and identification. *Anal Chem* **78**, 779–787 (2006).
79. Benton, H. P., Want, E. J. & Ebbels, T. M. D. Correction of mass calibration gaps in liquid chromatography-mass spectrometry metabolomics data. *Bioinformatics* **26**, 2488–2489 (2010).
80. Tautenhahn, R., Böttcher, C. & Neumann, S. Highly sensitive feature detection for high resolution LC/MS. *BMC Bioinformatics* **9**, 504 (2008).
81. Kuhl, C., Tautenhahn, R., Böttcher, C., Larson, T. R. & Neumann, S. CAMERA: An Integrated Strategy for Compound Spectra Extraction and Annotation of Liquid Chromatography/Mass Spectrometry Data Sets. *Anal Chem* **84**, 283–289 (2012).
82. Collins, J. R., Edwards, B. R., Fredricks, H. F. & Van Mooy, B. A. S. LOBSTAHS: An Adduct-Based Lipidomics Strategy for Discovery and Identification of Oxidative Stress Biomarkers. *Anal Chem* **88**, 7154–7162 (2016).
83. Melamud, E., Vastag, L. & Rabinowitz, J. D. Metabolomic Analysis and Visualization Engine for LC−MS Data. *Anal Chem* **82**, 9818–9826 (2010).
84. Clasquin, M. F., Melamud, E. & Rabinowitz, J. D. LC-MS Data Processing with MAVEN: A Metabolomic Analysis and Visualization Engine. *Curr Protoc Bioinformatics* **37**, 14.11.1-14.11.23 (2012).
85. Wang, M. *et al.* Sharing and community curation of mass spectrometry data with Global Natural Products Social Molecular Networking. *Nat Biotechnol* **34**, 828–837 (2016).

86. Wang, F. *et al.* CFM-ID 4.0: More Accurate ESI-MS/MS Spectral Prediction and Compound Identification. *Anal Chem* **93**, 11692–11700 (2021).
87. Watrous, J. D. *et al.* Directed Non-targeted Mass Spectrometry and Chemical Networking for Discovery of Eicosanoids and Related Oxylipins. *Cell Chem Biol* **26**, 433-442.e4 (2019).
88. Tsugawa, H. *et al.* A lipidome atlas in MS-DIAL 4. *Nat Biotechnol* **38**, 1159–1163 (2020).
89. Lamborg, C. H. *et al.* The flux of bio- and lithogenic material associated with sinking particles in the mesopelagic 'twilight zone' of the northwest and North Central Pacific Ocean. *Deep Sea Res 2 Top Stud Oceanogr* **55**, 1540–1563 (2008).
90. Collins, J. R. *et al.* The multiple fates of sinking particles in the North Atlantic Ocean. *Global Biogeochem Cycles* **29**, 1471–1494 (2015).
91. Whiteside, J. H. *et al.* Pangean great lake paleoecology on the cusp of the end-Triassic extinction. *Palaeogeogr Palaeoclimatol Palaeoecol* **301**, 1–17 (2011).
92. Iacazio, G., Langrand, G., Baratti, J., Buono, G. & Triantaphylides, C. Preparative, Enzymatic Synthesis of Linoleic Acid (13S)-Hydroperoxide Using Soybean Lipoxygenase-1. *J. Organic Chem* **55**, 1690–1691 (1990).
93. Landry, M. R. & Hassett, R. P. *MARINE BIOLOGY Estimating the Grazing Impact of Marine Micro-Zooplankton *. Marine Biology* vol. 67 (1982).
94. Bartual, A., Morillo-García, S., Ortega, M. J. & Cózar, A. First report on vertical distribution of dissolved polyunsaturated aldehydes in marine coastal waters. *Mar Chem* **204**, 1–10 (2018).
95. Bartual, A. *et al.* Polyunsaturated aldehydes from large phytoplankton of the Atlantic Ocean surface (42°N to 33°S). *Mar Drugs* **12**, 682–699 (2014).
96. Fontana, A. *et al.* Chemistry of oxylipin pathways in marine diatoms. *Pure and Applied Chemistry* **79**, 481–490 (2007).
97. d'Ippolito, G. *et al.* New C16 fatty-acid-based oxylipin pathway in the marine diatom Thalassiosira rotula. *Org Biomol Chem* **3**, 4065–4070 (2005).
98. D'Ippolito, G. *et al.* 15S-Lipoxygenase metabolism in the marine diatom Pseudo-nitzschia delicatissima. *New Phytologist* **183**, 1064–1071 (2009).
99. Lauritano, C. *et al.* Effects of the oxylipin-producing diatom Skeletonema marinoi on gene expression levels of the calanoid copepod Calanus sinicus. *Mar Genomics* **24**, 89–94 (2015).

Supplemental Information

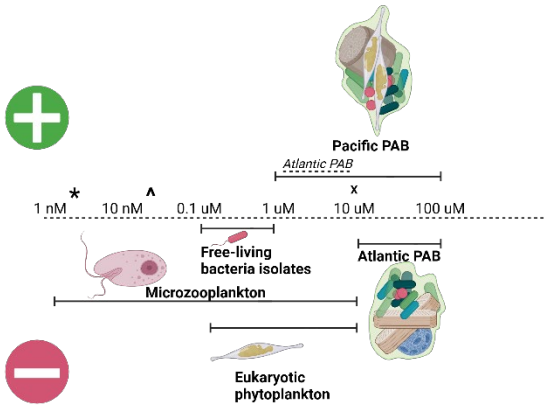

Figure S1. A summary of the range of concentrations known to be bioactive in amendment experiments and the maximum concentrations observed across the global ocean. The asterisk is the highest dissolved PUA concentration observed *in situ.*[94]. The caret is the highest particulate PUA concentration observed *in situ*[94]. The 'x' is the highest PUA concentration observed within sinking particles[35].

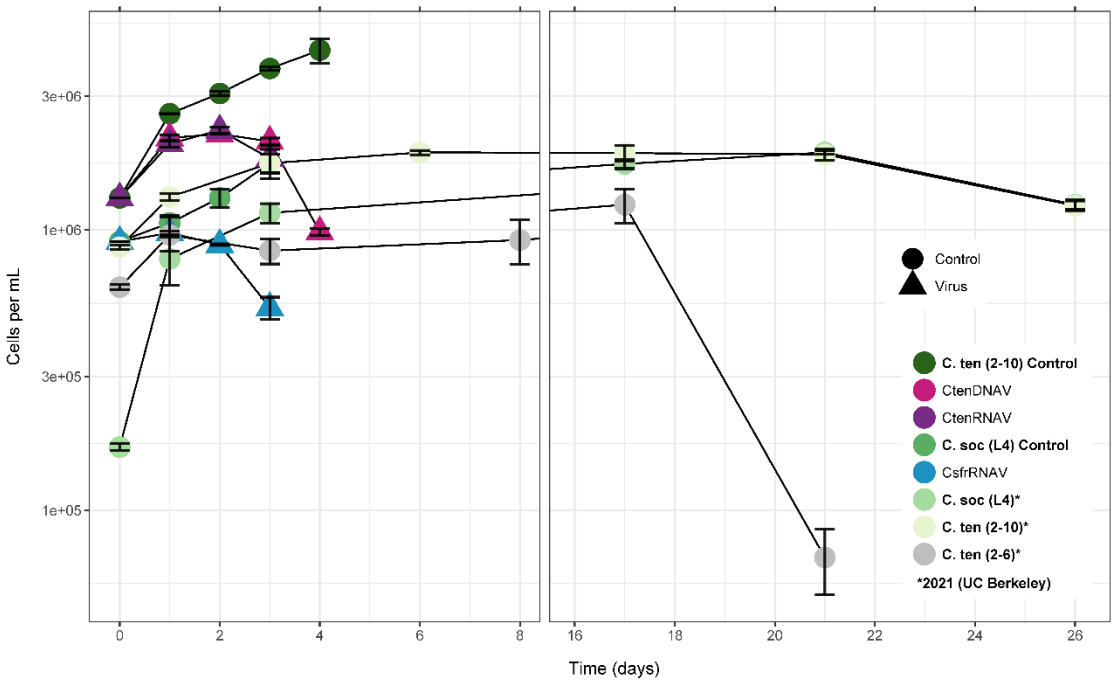

Figure S2. Time course of virus infection of *C. tenuissimus* and *C. socialis*. Growth curves for uninfected host-only control triplicates (green circles), *C. tenuissimus* infected with CtenRNAV (purple triangles) and CtenDNAV (pink triangle) viruses, and C. socialis infected with CsfrRNAV (blue triangles). Initial experiments at Rutgers in 2016 followed the diatom hosts, *Chaetoceros socialis* L4 (grass green circles) and *Chaetoceros tenuissimus* 2-10 (darkest green circle), to late exponential/ stationary phase and the dissolved lipid extracts were processed at WHOI. Subsequent experiments at UC-Berkely in 2021 followed cells well into stationary and decline phase (mint green, light green, and grey circles, denoted by an asterisk in the legend) were analyzed at UC-Berkeley.

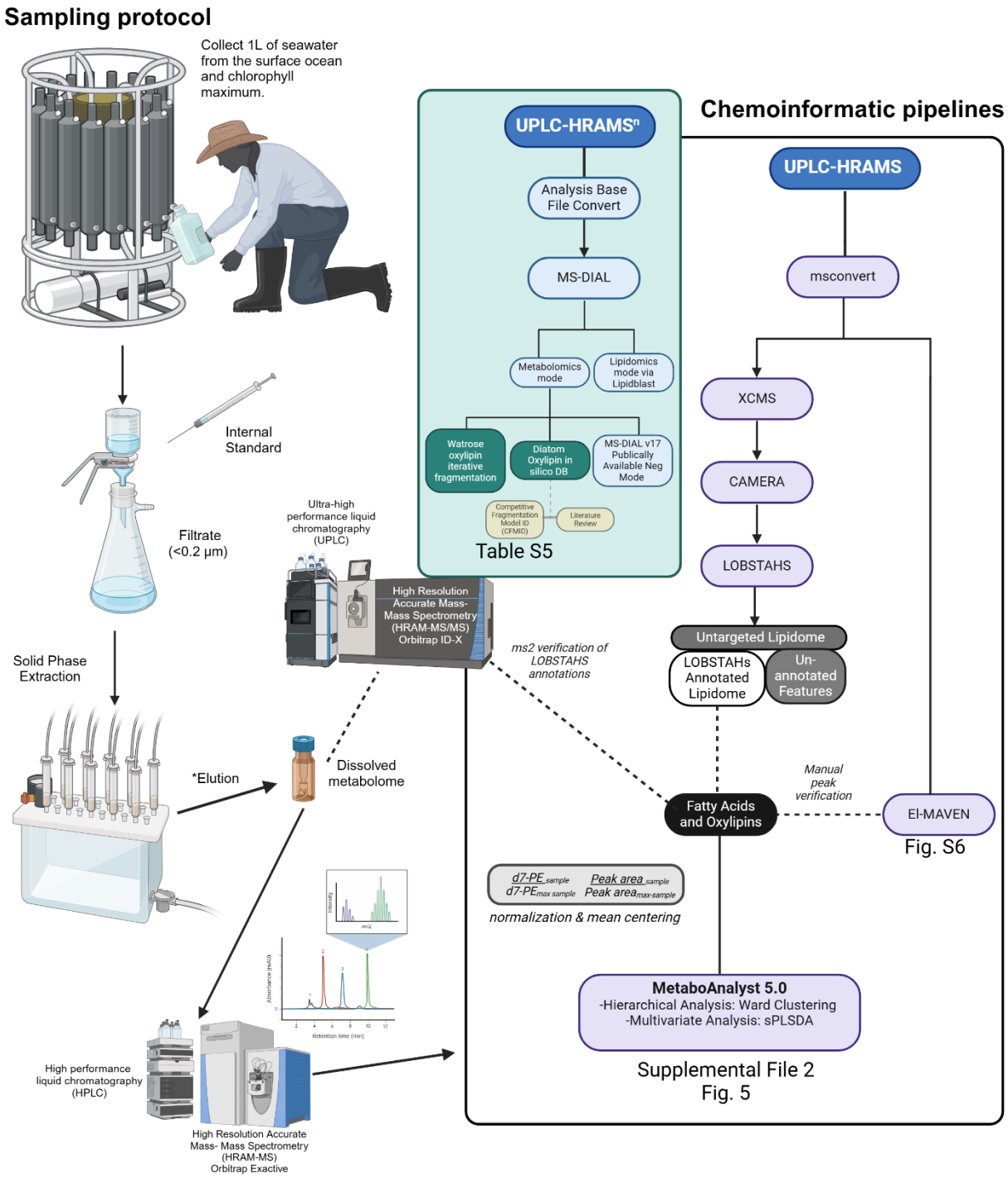

Figure S3. Outline of dissolved metabolome sampling at sea as well as sample extraction and analysis in the lab. One liter of water was collected from the surface ocean (55% I0 depth approx. 5 m) and the chlorophyll maximum (4-35 m) at each station. The 1L sample was filtered through a 0.2 um filter and benzaldehyde was added to the filtrate as an internal standard. The dissolved organics were extracted from the filtrate onto a Water HLB Solid Phase Extraction cartridge using a vacuum manifold. SPE Samples were flash frozen, and the dissolved metabolome was eluted from the SPE back in the lab. Dissolved metabolome samples were run for lipidomic analysis using HPLC paired with Orbitrap Exactive mass spectrometer in early 2014. Three samples were excluded from further analysis due to missing internal standard. The eleven remaining raw lipidomes were processed through the xcms-CAMERA-LOBSTAHS-MetaboAnalyst Chemoinformatic pipeline in the black box. Representative

samples were rerun in 2021 using an Orbitrap ID-X mass spectrometer which allowed for more targeted ms2 fragmentation for higher confidence oxylipin annotation of important features from the comparative statistical analysis provided by MetaboAnalyst; these annotations can be found in Table S5.

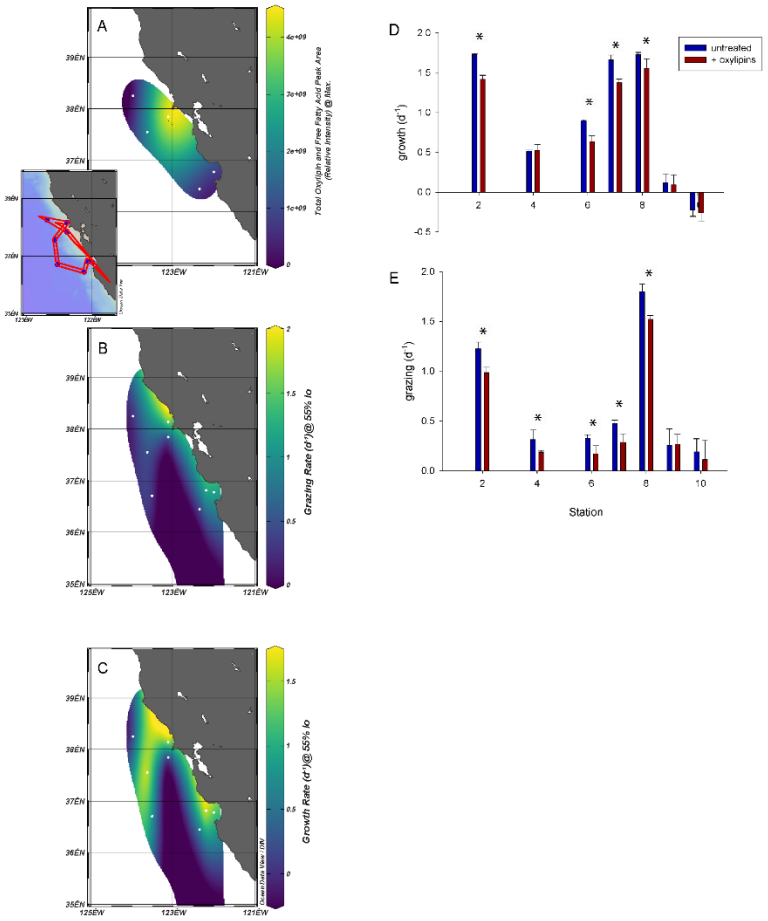

Fig S4. Grazing and growth were lowest at the station with the highest oxylipin concentration and deckboard amendment experiments with exogenous oxylipins show inhibition of growth and grazing. Contour maps of **A)** the maximum total oxylipin and free fatty acid peak area, **B)** microzooplankton grazing rate at the 55% I0 depth, and **C)** phytoplankton growth rate at the 55% I0 depth for each station of the DYEatom cruise. Plotted with Ocean Data View using the DIVA contouring model which accounts for general ocean current patterns. D) Grazing rate presented as a bar chart with the parallel oxylipin amendment rate. Asterisk denotes statistical difference in + oxylipin amendment from the control treatment. E) Growth rate presented as a bar chart with the parallel oxylipin amendment rate. Asterisks denote statistical difference from the control treatment.

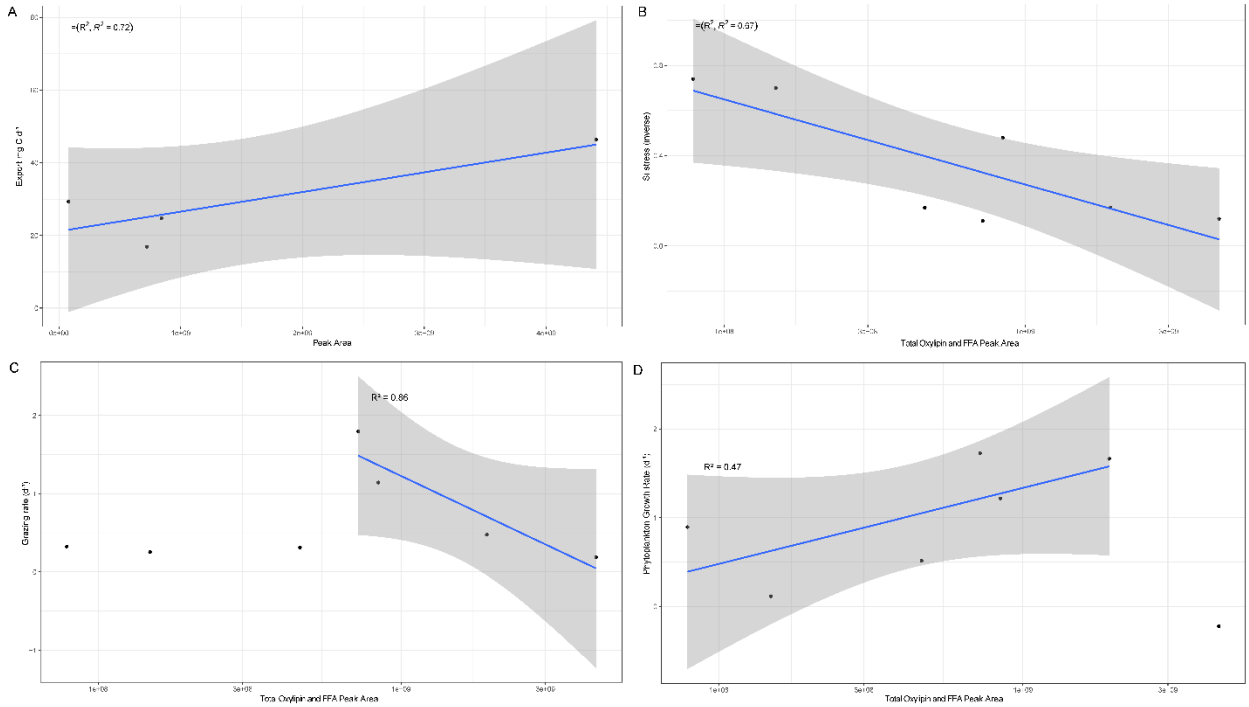

Fig S5. Relationship between the total peak area and **A)** export, **B)** Si-stress of the surface ocean community **C)** Grazing rate, and **D)** Phytoplankton growth rate across the DYEatom cruise (PS1312) reflect allelopathy of oxylipins on the community, oxylipin production under stress, and evidence of a link between oxylipin production and the viral shuttle. The silica stress metric is described in ref[17]. Briefly, the Y-axis is the percentage of the Si uptake rate (B) that happens in the ambient Si concentration vs. a deck-board amendment with exogenous Si. A lower value indicates more silicon stress in that environment. For the phytoplankton growth regression (D) all but the negative growth rate was included. And for the microzooplankton grazing rate regression (C) the low peak area samples were excluded.

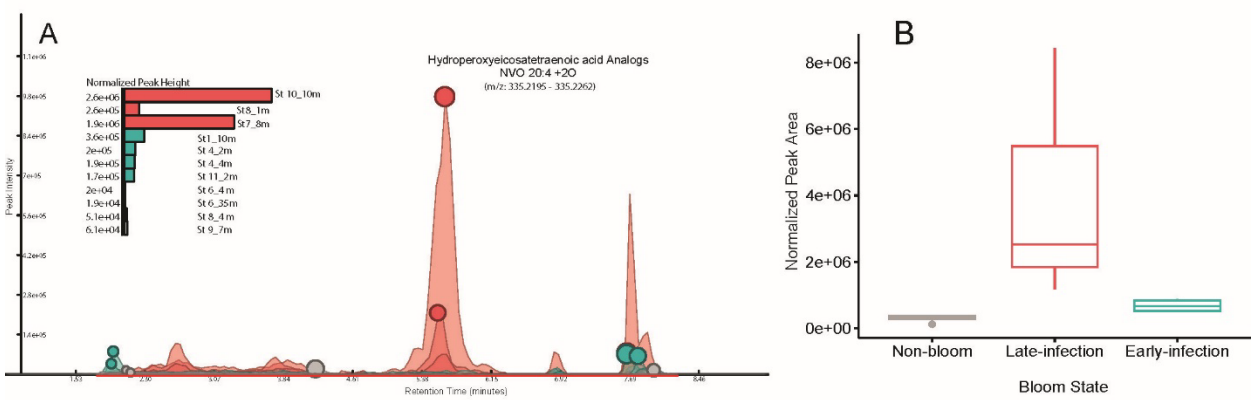

Figure S6. Analogs to the exogenous oxylipins found to be bioactive in Fig 6I-K were found *in situ* in addition to the various similar oxylipins of different carbon chain lengths and degrees of unsaturation highlighted in Fig 5. **A)** Extracted ion chromatogram of HpETE analogs (i.e. compounds with a $[M-H]^-$ adduct m/z of 335.2232) observed in the DYEatom dissolved meta-lipidome and the integrated peak height displayed in the inset bar charts. **B)** The normalized peak area for HpETE analogs averaged across each bloom state. Box plots show the 1st and 3rd quartile range as the upper and lower bounds of the box and the mean is denoted as a line through the box. The error bars denote the standard deviation with the dots representing outliers.

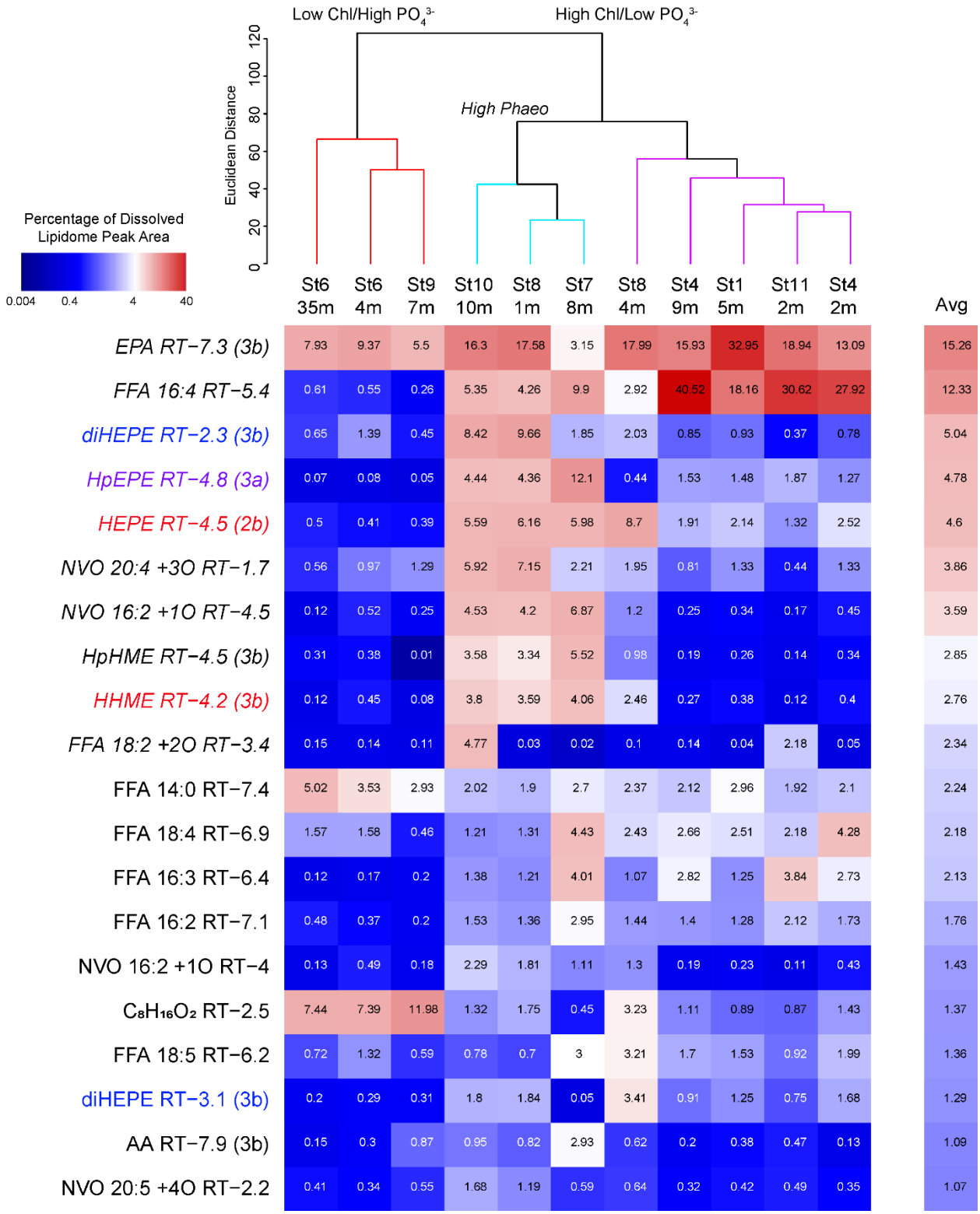

Figure S7. Features representing greater than 1% of the peak area in the annotated dissolved meta-lipidome on average. The heat map displays the percentage of the total annotated peak area attributable to each molecular species across the samples. Samples are grouped by similarity profile analysis of the structure of the dissolved meta-lipidome across the cruise track as presented in Fig. 5A.

1013
1014
1015
1016
1017
1018

Table S1. Compilation of maximum PUA and NVO concentrations observed in situ. Each oxylipin subclass is broken down into particulate (p-prefix) and dissolved (d-prefix). Note that no dNVO quantifications have been published. The pPUA values are derived from sonicated or freeze-thawed cells that were collected on a filter presenting a potential oxylipin concentration. The dPUA values were collected by extracting the organics on to a solid phase extraction cartridge. The pNVO values in Mar 2005 and April 2011 were estimated from cell abundances and fg of oxylipin per cell.

Oceanic Region	Date	pPUA	dPUA	pNVO	dNVO	$PUA_{sinking/suspended}$	Citation
Adriatic	Mar 2005			1.76 nM			Ianora *et al.*, 2015[8]
	Mar 2006	9 nM	2.3 nM				Vidoudez *et al.*, 2011[38]
	Feb 2008	20 nM	0.1 nM				Ribalet *et al.*, 2014[23]
	April 2011			48 pM			Lauritano *et al.*, 2016[10]
	June 2017			1.75 nM			Russo *et al*, 2020[25]
	Avg 2017			0.4 nM			
Pearl River Estuary	June 2015	20 nM	0.37 nM				Wu…Luo, 2021a[39]
	June 2019	0.2 nM	0.1 nM			10 µM	Wu...Dong, 2021b [34]
Western Mediterranean	Aug 2011	1.65 nM	1.87 nM				Bartual *et al.*, 2018[94]
	Mar 2012	0.2 nM	0.54 nM				
	Oct 2015	5.3 pM	34.9 pM				
North Atlantic	July 2011	1 pM					Bartual *et al.*, 2014[95]
	Jun 2012					37 µM	Edwards *et al.*, 2015[35]

1019
1020

Table S2. Authentic fatty acid, polyunsaturated aldehyde, non-volatile oxylipin standards with the common name or abbreviation, the structural level annotation assigned by the lipidomics pipeline presented here, and the retention time (RT) of each compound. Comparisons to the RT of the authentic standards were used to assign putative annotations to features in the dissolved lipidome.

Authentic Standard	Common Abbreviation/ Name	Structural Level Annotation	RT
Octanoic acid	--	FFA 8:0	2.65
Arachidonic acid	AA	FFA 20:4	8.09
Docosahexaenoic acid	DHA	FFA 22:6	7.71
9-Hydroperoxy octadecadienoic acid	9-HpODE	NVO 18:2 2O	5.44
13-Hydroperoxy octadecadienoic acid	13-HpODE	NVO 18:2 2O	5.44
9-Hydroxy octadecatrienoic acid	9-HOTrE	NVO 18:3 1O	4.02
13-Hydroperoxy octadecatrienoic acid	13-HpOTrE	NVO 18:3 2O	4.65
9-Hydroperoxy octadecatrienoic acid	9-HpOTrE	NVO 18:3 2O	4.28
15-Hydroxy eicosatrienoic acid	15-HETrE	NVO 20:3 1O	6.11
15-Hydroxy eicosatetraenoic acid	15-HETE	NVO 20:4 1O	5.43
5-Hydroperoxy eicosatetraenoic acid	5-HpETE	NVO 20:4 2O	5.01
12-Hydroperoxy eicosatetraenoic acid	12-HpETE	NVO 20:4 2O	5.93
15-Hydroperoxy eicosatetraenoic acid	15-HpETE	NVO 20:4 2O	5.73
5,6-Dihydroxy eicosatetraenoic acid	5,6-diHETE	NVO 20:4 2O	3.48
14,15- Dihydroxy eicosatetraenoic acid	14,15-diHETE	NVO 20:4 2O	3.00
5,12- Dihydroxy eicosatetraenoic acid	Leukotriene B4	NVO 20:4 2O	2.89
15-Hydroxy eicosapentaenoic acid	15-HEPE	NVO 20:5 1O	4.56
5,6,15- Trihydroxy eicosapentaenoic acid	Lipoxin A5	NVO 20:5 3O	1.72
Heptadienal	--	PUA 7:2	1.90
Octadienal	--	PUA 8:2	2.28
Nonadienal	--	PUA 9:2	2.69
Decadienal	DD	PUA 10:2	3.65

Table S3. Viral Infection and general death oxylipin-biomarkers from our *Chaetoceros*-virus experiments that were observed in culture, field studies, and their known allelopathy. The diatom species that each compound has been observed in is noted: *Skeletonema marinoi* (Sm), *Chaetoceros socialis* (Cs), *Chaetoceros affinis* (Ca)[96], *Thalassiosira rotul*[97] (Tr), *Pseudo-nitzchia delicatissima* (Pd)[98], *Skeletonema pseudocostatum* (Sp)[13], and *Phaeodactylum tricornutum* – microzooplankton grazing experiments (Pt-MZP)[33]. The lipidomic pipeline in this study automatically annotates to the structural level. Structural isomers of these compounds were observed in the DYEatom cruise dissolved lipidome (denoted as this study) and studies in the Mediterranean[8,10,25,99]. Compounds with known allelopathic effects are [10,25]. Many of these compounds were annotated to the function group level using a retention time model or *in silico* fragmentation model as outlined in Edwards *et al.* (2024); compound abbreviations in Fig 3B-C.

Viral Biomarkers	Observed in culture	Observed in the Field	Known allelopathy	RT-model	CFMID model
FFA 14:2 +1O_mz_239.165_RT_1.71	isomer Pt-MZP		*MZP grazing*		
FFA 20:5 +2O_mz_333.2073_RT_2.08	Sm, Ca, isomer Pt-MZP		Copepods; 20:4 +2O dihydro and hydroperoxy decrease MZP grazing; HpETE modulate particle associated microbial activity (this study)	10,11-diHEPE	
FFA 16:3 +3O_mz_297.1708_RT_2.13	16:3 oxylipins general Sm, Tr				
FFA 14:2 +1O_mz_239.165_RT_2.56	isomer Pt -MZP		*MZP grazing*		
FFA 16:3_mz_249.1857_RT_7.36	16:3 oxylipins general Sm, Tr	Lauritano *et al.,* 2016			
FFA 22:5 +1O_mz_345.2436_RT_7.67	*Lepidocylindrus*	Lauritano *et al.,* 2016; Russo *et al.,* 2020; this study	*Copepods*		
FFA 14:2 +1O_mz_239.165_RT_2.25	isomer Pt -MZP		*MZP grazing*		
FFA 22:4 +1O_mz_347.2593_RT_7.77	*Lepidocylindrus*				
FFA 18:3 +2O_mz_309.2074_RT_5.01	cyanobacteria, green algae, moss				
FFA 20:4 +1O_mz_319.2279_RT_5.95	Tr, *Stephanopyxis turris*, red algae, fungi	Lauritano *et al.* 2016; Russo *et al.* 2020; this study	Copepods; analog impacts sea urchins		

Death Biomarkers	Observed in culture	Observed in the Field	Known allelopathy	RT-model	CFMID model
FFA 16:1 +1O_mz_269.2123_RT_4.37	Sm, Tr	Lauritano *et al.* 2016; this study	Copepods		
FFA 18:3 +2O_mz_309.2073_RT_1.98	cyanobacteria, green algae, moss				
FFA 16:2 +1O_mz_267.1966_RT_4.78	Sm, Tr	this study	Copepods	9-KHME	9-epHME
FFA 16:3 +3O_mz_297.1707_RT_1.52	16:3 oxylipins general Sm, Tr				
FFA 16:2 +1O_mz_267.1966_RT_4.28	Sm, Tr	this study	Copepods	9-KHME	5-epHME
FFA 16:3 +1O_mz_265.1809_RT_2.99	Sm, Tr	Lauritano *et al.* 2016; Russo *et al.* 2020; this study	Copepods		9-HHTrE
FFA 16:2 +1O_mz_267.1966_RT_3.46	Sm, Tr, Flowering plants	this study	Copepods	9-KHME	
FFA 18:4 +1O_mz_291.1967_RT_2.02					
FFA 18:3 +2O_mz_309.2073_RT_7.32	cyanobacteria, green algae, moss				
FFA 16:4 +2O_mz_279.1602_RT_1.85	Sm	this study	Copepods		9-HpHTE

Table S4. Location and data of collection for the dissolved meta-lipidomic samples across the DYEatom cruise track

Station	**Depth (m)**	Latitude N	Longitude W	Date	MLD
1	10	36°46.864 '	121°59.1257 '	June 27, 2013	7
4	2	36°27.31 '	122°20.32 '	June 29, 2013	16
4	4	36°27.31 '	122°20.32 '	June 29, 2013	16
6	4	36°42.61 '	123°29.62 '	June 30, 2013	26
6	35	36°42.61 '	123°29.62 '	June 30, 2013	26
7	8	37°33.42 '	123°37.96 '	July 1, 2013	18
8	1	38°8.96 '	123°5.95 '	July 2, 2013	7
8	4	38°8.96 '	123°5.95 '	July 2, 2013	7
9	7	38°15.89 '	123°58.12 '	July 3, 2013	27
10	10	37°50.24 '	123°6.6 '	July 4, 2013	10
11	2	36°46.67 '	121°58.83 '	July 5, 2013	11

Table S5. Further annotation of significant compounds identified by sPLS-DA analysis of either lysis or mid infection within the DYEatom cruise dissolved lipidome. LOBSTAHS annotation, peak retention time, the mass to charge ration (m/z) of the feature, and the annotation from considering the ms^2 fragmentation of samples analyzed using HRAM-MS^n analysis outlined in Fig. S3. It is also noted whether each compound was a biomarker observed in the *Chaetoceros* culture experiments in Fig. 3B-C and whether the compound has known allelopathy (based on the studies cited in Table S3).

Lysis	LOBSTAHS annotation	Retention Time (min)	m/z	Further Annotation	Annotation Method	Biomarker/ Allelopathic
	PUA 12:5 1O	2.5	189.0921	$C_{12}H_{14}O_2$	-	No/No
	FFA 20:4 +3O	4.1	351.2177	5-epoxy 8,14 dihydroxy eicosatrienoic acid	hypothesized from Edwards Lab DB	No/No
	FFA 22:5 +1O	6	345.2435	signal too low	-	No/No
	FFA 16:1 +1O	4.2	269.2122	9-HHME	Edwards Lab DB	Death/Yes
	FFA 20:4 +4O	4.5	367.2126	signal too low	-	No/No
	FFA 20:4 +1O	5.4	319.2279	signal too low	-	Virus/Yes
	FFA 16:2 +1O	4	267.1966	9-oxoHME	Edwards Lab DB	Death/Yes
	FFA 20:5 +1O	4.5	317.2122	14-HEPE	Edwards Lab DB	No/Yes
	FFA 16:1 +2O	4.5	285.2071	9-HpHME	Edwards Lab DB	No/No
	FFA 16:2 +1O	4.5	267.1966	9-HHDE	Edwards Lab DB	Death/Yes
Mid Infection	**LOBSTAHS annotation**	**Retention Time (min)**	**m/z**	**Further Annotation**	**Annotation Method**	
	FFA 22:5 +4O	2.6	393.2283	signal too low	-	No/No
	FFA 22:4 +4O	3.2	395.2439	signal too low	-	No/No
	FFA 22:4 +4O	3.7	395.2439	signal too low	-	No/No
	FFA 22:5 +4O	4.2	393.2283	signal too low	-	No/No
	FFA 22:4 +4O	4.2	395.2439	signal too low	-	No/No
	FFA 22:4 +4O	2.7	395.2439	signal too low	-	No/No
	FFA 22:5 +4O	3.7	393.2283	signal too low	-	No/No
	FFA 22:5 +4O	3.3	393.2283	signal too low	-	No/No
	FFA 16:4	5.4	247.1704	hexadecatetraenoic acid	MS-Dial Lipid Blast	No/No
	FFA 18:4 +2O	5.4	307.1915	signal too low	-	No/No

1067
1068
1069
1070

Table S6. Average richness and diversity of the oxylipins and free fatty acids in the dissolved lipidome collected from the surface ocean along the DYEatom cruise. Samples subdivided by the state of diatom infection.

Non-bloom			
Samples	Richness	Diversity	Sum
St6_4m	165	-4.03134	$2x10^8$
St6_35m	164	-3.97726	$1.28\ x10^8$
St9_7m	156	-3.92887	$3.25\ x10^8$
Avg	*161.6667*	*-3.97915*	*2.17* $x10^8$
stdev	*4.932883*	*0.051261*	*99692081*
Post-Lytic			
Samples	Richness	Diversity	Sum
St7_8m	175	-3.60247	$5.27\ x10^9$
St8_1m	175	-3.47831	$2.31\ x10^9$
St8_4m	174	-3.74992	$3.74\ x10^9$
St10_10 m	174	-3.54632	$1.4\ x10^{10}$
Avg	*174.5*	*-3.59426*	*5.48* $x10^9$
stdev	*0.57735*	*0.115527*	*6* $x10^9$
Active Infection			
Samples	Richness	Diversity	Sum
St11_2m	174	-2.94217	$2.62\ x10^9$
St4_2m	174	-3.28648	$1.37\ x10^9$
St1_5m	175	-2.94248	$2.17\ x10^9$
St4_9m	172	-2.71614	$1.96\ x10^9$
Avg	*173.75*	*-2.97182*	*2.03* $x10^9$
stdev	*1.258306*	*0.235316*	*5.18* $x10^8$

Table S7. T-test results showing a significant difference between the average diversity of the dissolved lipidome collected during three different states of viral infection. Bold italics values are significant <0.01, bold values are significant <0.05 with a Bonferroni correction.

	Richness	Diversity	Sum
Post-lytic *vs.* Non-bloom	0.044609	***0.003134***	0.177903
Active Infection *vs.* Post-lytic	0.336716	**0.007219**	0.334421
Active Infection *vs.* Non-bloom	0.045554	***0.002336***	**0.004728**

Supplemental File 1: Dissolved Lipidome Rutgers *Chaetoceros* Viral Infection Experiments
Supplemental File 2: Dissolved Meta-Lipidome DYEatom Cruise.
Supplemental File 3: DYEatome Cruise Lipidome Retention Time Model